Dynamics and subcritical transition focusing on spatially-localized turbulence in two-dimensional Kolmogorov flow

Yoshiki Hiruta

January 23, 2019

Contents

Abstract

Fluid flows are ubiquitous in our daily life. We already know the governing law of fluid flow in the scale of our daily life, Navier-Stokes equations, but prediction and control of turbulent flow and turbulence transition is still difficult.

In this thesis, understandings of dynamics and turbulence transition for the subcritical regime are developed where spatially-localized turbulence plays a key role. For the subcritical regime, where no unstable mode exists around the laminar solution, spatially-localized turbulence, such as a spot in channel flow and puff in pipe flow, are widely observed for laboratory and numerical experiment. Dominant modes are unknown for this case while unstable modes of the linear theory are generally dominant for the subcritical regime. Localization in spatial direction should lead scale separation of length scale comparing to system size and that scale separation makes theoretical and numerical approach difficult. The basic finding of this thesis is that the uniform flow perpendicular to forcing direction makes the laminar solution stable. Kolmogorov flow is simple and more uniform than wall-bounded flow. We are able to investigate subcritical flow at low cost. In main parts of the thesis, two different cases with time scale separation are discussed. At the first part, intermittent direction reversal of spatially-localized turbulence is found. Spatially-localized turbulence moves with constant speed on average, and it changes its own moving direction suddenly and intermittently. We discuss the relationship between the chaotic dynamics of inner freedoms and direction reversals. The second topic is subcritical turbulence transition. A new example of subcritical turbulence transition governed by two-dimensional Navier-Stokes equation without material walls. Theoretical estimation yields that critical Reynolds number of linear theory blows up to infinity at a finite flow rate perpendicular to forcing. Confirmed by numerical integration, the number of spatially-localized turbulences changes randomly

introducing a large drag forcing. The results also suggest subcritical transition belongs to the directed percolation universality class.

Acknowledgement

First of all, I would like to express deep thanks to Professor Sadayoshi Toh, who is my supervisor of the Ph.D. course of science at Kyoto University. He has supported my research and has given a lot of valuable comments. I also would thank his insightful suggestions and great tolerance. I am grateful to Professor Takeshi Matsumoto. His comments and advice help my college life as well as my research.

I would also like to thank my colleagues of Fluid physics group of Kyoto University, Kentaro Takagi, Toshiki Teramura, Shunsuke Akita, Naohiro Temmoku, Ryo Murakami, Tin Unkai, Tatsuro Kishi, Michinori Sato, Takafumi Maruishi, Yo Yamada, Ryo Sakai for their discussion, advice, and suggestion. I would like to thank the members of Research Group for Fluid dynamics in Research Institute for Mathematical Sciences(RIMS), Kyoto University, for their advice and comments.

A part of works in this thesis was supported by JSPS KAKENHI Grant Number JP18J13334, Grant-in-Aid for JSPS Research Fellow; the Research Institute for Mathematical Sciences, a Joint Usage/Research Center located in Kyoto University.

Finally, I give a special thanks to my family for their support throughout my life.

Chapter 1

General introduction

1.1 Nonuniform turbulence

Fluid flows are ubiquitous not only in our daily life but also in phenomena from quantum to cosmic scales. In macroscopic scale that is typically larger than the size of molecules, flows are described by the following hydrodynamic equations[Lam45, LL59]:

$$\partial_t \rho + \partial_j (u_j \rho) = 0, \tag{1.1}$$

$$\partial_t \rho u_i + \partial_j (u_j \rho u_i) = \partial_j \sigma_{ji} + f_i. \tag{1.2}$$

The former is the conservation law of mass and the latter is Newton's equation of motion. Here, ρ and $\boldsymbol{u}$ are the density and the velocity field of fluid, and σ and $\boldsymbol{f}$ denote the stress tensor and the external body force, respectively. In this macroscopic description, fluid is regarded as continuous media, and each spatial point of the hydrodynamic equations contains a huge number of molecules. These equations are partial differential equations and solutions of the equations describe the behavior of fluid under appropriate boundary conditions. However, it is difficult to obtain general solutions and further to elucidate their character because of its nonlinearity. For the motion of fluids in our daily scale, it is often sufficient to impose incompressibility ($\partial_t \rho + u_j \partial_j \rho = 0$) and to regard the fluid as Newtonian fluid ($\sigma_{ij} = -\rho P \delta_{ij} + \rho\nu(\partial_j u_i + \partial_i u_j)$). Then, the Navier-Stokes equations with

constant ρ

$$\partial_t \boldsymbol{u} + (\boldsymbol{u} \cdot \boldsymbol{\nabla})\boldsymbol{u} = -\boldsymbol{\nabla} P + \nu \nabla^2 \boldsymbol{u} + \boldsymbol{f}, \tag{1.3}$$

$$\boldsymbol{\nabla} \cdot \boldsymbol{u} = 0, \tag{1.4}$$

are sufficient for describing fluid phenomena. Here, P is the pressure function, and its behavior is not affected by thermodynamic quantities but determined by the velocity field. The pressure function is considered as an undetermined function corresponding to the constraint of incompressibility (1.4). Then, Eqs. (1.3) and (1.4) determine the time evolution of the dependent variables, $\boldsymbol{u}$. The kinematic viscosity, ν which reflects the microscopic structure of the fluid is the only parameter of the Navier-Stokes equations.

It is generally difficult to fully understand fluid phenomena despite the superficial simplicity of the equations (1.3) and (1.4). For example, when Reynolds number which is non-dimensionalized momentum of the fluid and denoted by Re is large enough, a highly complex solution called "turbulence" is realized[Fri95]; Turbulence is spatiotemporally nonuniform and its kinetic energy is distributed among the wide range of scales. This tendency is also seen in laboratory experiments.

One of the ultimate goals of fluid physics is to elucidate turbulence based on the governing equations. Turbulence theories on statistically isotropic and homogeneous turbulence have achieved a certain measure of success in recent years based on the universality of small scale behavior. However, fluid flows in scientific interest and practical use of engineering are often anisotropic. In fact, recent precise numerical experiments on turbulence at high Reynolds number reveal even symmetry breaking transient flows sustained for a long time. Although practical theories such as turbulence modelings, which are usually based on the ideas that smaller scales are universal and thus seemed to be slaved by larger scales, have been developed, they do not necessarily work in elucidating more realistic turbulence so far, to our knowledge. In this situation, therefore, a novel approach is required to deal with nonuniform turbulence.

1.1.1 Turbulence Transition

As mention above, turbulence is realized at relatively high Reynolds number. In contrast, at sufficiently low Reynolds number we obtain a laminar solution, which is a stationary linear solution of the Navier-Stokes equations

for parallel flows[Fri95, DG95]. Since turbulence has high energy dissipation, efficient diffusion and anomalous mixing, the estimation of Reynolds number at which the transition from the laminar state to turbulence occurs, is important for practical use of fluid; if it does, the value is called the critical Reynolds number, Re_c[Rey83]. Recent years approaches based on statistical physics become effectively available as well as bifurcation theory of dynamical system.

View from dynamical system

An important indicator of turbulence transition is linear stability of the laminar state as dynamical systems. From the viewpoint of dynamical systems, the time evolution of the velocity, $\boldsymbol{u}$, is considered as the motion of a point in phase space or state space. Especially for time-independent external force and boundary conditions, it is an autonomous dynamical system. Let $\boldsymbol{X}$ be an element of the phase space and evolve by the following equation

$$\frac{d\boldsymbol{x}}{dt} = \boldsymbol{F}(\boldsymbol{X}). \tag{1.5}$$

In this case, a laminar solution is a fixed point, $\boldsymbol{X}_0$, that satisfies $\boldsymbol{F}(\boldsymbol{X}_0) = 0$ while turbulence states are complex motion in phase space. Around $\boldsymbol{X}_0$, an infinitesimal disturbance $\delta\boldsymbol{X} = \boldsymbol{X} - \boldsymbol{X}_0$ follows

$$\frac{d\delta\boldsymbol{x}}{dt} = D\boldsymbol{F}(\boldsymbol{X}_0)\delta\boldsymbol{X} + \mathcal{O}(|\delta\boldsymbol{X}|^2), \tag{1.6}$$

where $D\boldsymbol{F}(\boldsymbol{X}_0)$ is the linearized operator around $\boldsymbol{X}_0$. The fixed point is linearly unstable when the spectrum of $D\boldsymbol{F}(\boldsymbol{X}_0)$ contains eigenvalues with positive real parts. If the laminar solution is linearly unstable, such the state is broken by even an infinitely small perturbation in the phase space and the laminar solution is no longer stably observed in the physical space. We set the lower bound of linearly unstable Reynolds number as Re_l. Supercritical scenario for turbulence transition has introduced in the middle of twenty century. In this scenario, the cascade of bifurcation adds the degree of freedom step by step along with the complexity of attracting sets. This critical Reynolds number denoted by Re_l is the upper bound of Re_c. In general, the parameter region above this critical value ($\mathrm{Re}\geq\mathrm{Re}_l$) is called supercritical while the parameter region below the critical ($\mathrm{Re}\leq\mathrm{Re}_l$) is called subcritical. Moreover, one can prove that there exists another upper bound denoted by

Re_g below which any perturbations decay exponentially for large class of Navier-Stokes equations (1.3) and (1.4). Thus, the relation

$$\mathrm{Re}_g \leq \mathrm{Re}_c \leq \mathrm{Re}_l \tag{1.7}$$

holds. For the supercritical region, the first unstable mode is crucial to describe phenomena. Weakly nonlinear stability theory or the method of amplitude equation is based on this idea. However, dynamics for the subcritical region has only a few clues which can select dominant modes. Especially for wall-bounded flows such as pipe and channel flows, Re_l is very large or infinite so that laminar-turbulence transition occurs subcritically. Unknown important modes prevent us from understanding subcritical transition unlike the supercritical case.

View from statistical physics

From laboratory and numerical observations, the spatial structure of turbulence at the onset subcritical transition tends to be spatially localized and embedded in the laminar state. This spatially localized turbulent state (SLT) is called turbulent puffin pipe flow and a turbulent spot in channel flow. Oblique turbulence patterns are also observed in Couette flow both in concentric cylinder and parallel plates[Col65, DSH10, TB11]. The spot and stripe patterns are composed of so-called streak structures which are identified as the dynamics of "minimal flow" in the modern sense: The details will be explained later. From the locality of dynamics, the following viewpoints arise in comparison with globally occupied turbulence.

(a) (probabilistic) "expansion" of turbulent region or "splitting" of turbulent state

(b) (probabilistic) "shrinking" of turbulent region or "decay" of turbulent state

(c) Moving of the center of SLT

(d) Interaction among other turbulent states

Considering the cases (a) and (b), the area occupied by an SLT can change in time as if they are stochastic though the governing equations are deterministic. For pipe flow, turbulence puffs split or decay. The basic idea for this

type subcritical transition is that turbulence is sustained when the splitting probability, p, is larger than the decaying probability, q, ($p > q$) while the laminar state is realized when $p < q$. We can expect p becomes larger and q becomes smaller for larger Reynolds number, and Reynolds number satisfying $p(\mathrm{Re}) \sim q(\mathrm{Re})$ should be critical Reynolds number Re_c[AMdL$^+$11]. This type of transition is caused by not dynamic but essentially statistical nature in contrast with the case of supercritical transition which is triggered by an exchange of the stability of the corresponding fixed point. Important characteristics of the subcritical transition of this type are

(i) Once the laminar state is spatially-globally realized, laminar state sustains after that.

(ii) New spatially-localized turbulent states arise around a turbulent state.

The former corresponds to linear stability. The latter means that an elementary process is spatially localized. Here, one can expect that the transition belongs to directed percolation (DP) universality class[Hin00]. DP universality class is a representative class of an absorbing state phase transition which is the phase transition between absorbing state and active state such that a whole state does not change once all of the states become the absorbing state. Contact process directed percolation and other models in various fields belong to DP universality class. In this context, each of an absorbing state and an active state corresponds laminar state and SLT, respectively. Recent experiments showed that the critical exponents of laminar-turbulence transition of wall-bounded flow match those of DP universality class. Essentially reaction-diffusion models resemble the dynamics of wall-bounded flow and coupled map lattice (CML) models also show DP class transition[CM88, Bar11].

Expectation of Directed Percolation universality class

Around the critical point of statistical phase transition, one can expect that macroscopic properties are independent of microscopic properties but depend on the spatial dimension, symmetry, and conserved quantities. Considering that physical quantity A is observed in length scale x and time scale t,d the system is parametrized by c, and the critical value of c is set 0 without loss of generality. The following scaling relations based on self-similarity are supposed in that the phenomenon is invariant under the following transfor-

mation,

$$c \to bc, \tag{1.8}$$
$$x \to b^{y_x} x, \tag{1.9}$$
$$t \to b^{y_t} t, \tag{1.10}$$
$$A \to b^{y_A} A, \tag{1.11}$$

where b is a constant and y_* denotes the scaling exponent for each variable. Then, the function form of the physical quantity A should satisfy the following one parameter relation with respect to b:

$$A(x, t, c) = b^{y_A} A(b^{y_x} x, b^{y_t} t, bc). \tag{1.12}$$

This relation can be utilized to predict the parameter dependence of various quantities around the critical point. For example, the spatiotemporal average of the quantity A denoted by $\bar{A}$ which depends only on c is written as follows:

$$\bar{A} = c^{-y_A} C \propto c^{-y_A}. \tag{1.13}$$

Here, $b = 1/c$ and $C = \bar{A}(c = 1)$. The actual value of y is generally unknown but can be deduced with relations such as symmetry as mentioned above.

For critical phenomena belonging to DP universality class, the order parameter ρ which takes zero for the absorbing state is a fundamental observable. The spatiotemporal average of ρ, $\bar{\rho}$, and ρ's correlation lengths both for temporal and spatial directions, $\xi_\parallel$ and $\xi_\perp$, are the fundamental set of physical quantities characterizing the critical phenomena. They should have the following parameter dependence:

$$\bar{\rho} \propto c^{\beta}, \tag{1.14}$$
$$\xi_\parallel \propto c^{\nu_\parallel}, \tag{1.15}$$
$$\xi_\perp \propto c^{\nu_\perp}. \tag{1.16}$$

These independent critical exponents also depend on spatial dimension. For higher spatial dimensions larger than $d = 4$, the critical exponents will agree with those obtained by mean field theory, $(\beta, \nu_\parallel, \nu_\perp) = (1, 1/2, 1)$, while the critical exponents will not be simple rational numbers, e.g. $(\beta, \nu_\parallel, \nu_\perp) \sim (0.276, 1.10, 1.73)$ for $d = 1$[Jen96]. For turbulence case, one can expect that ρ corresponds to turbulence fraction or occupation area of SLT.

1.1.2 Dynamics

Dynamics based on nonlinear modes

Since recent development of computer performance and numerical techniques enable us to directly observe the dynamics of turbulent motion, the idea or conjecture that the dynamics of turbulence confirmed for small systems is locally embedded even in a huge system has developed and become popular.

For example, the dynamics of so-called low-speed streak structure, self-sustaining process (SSP), which is widely identified as the near-wall dynamics in wall-bounded flows such as channel flow and boundary layer corresponds to or is similar to that of "minimal flow" turbulence. Here, the minimal flow is defined as the smallest system in which turbulent motion can be sustained. The dynamics in both of near-wall layer and minimal flow share the same characteristics, i.e., SSP that is the cyclic motion played by streaks, streamwise vortices and three-dimensional modes[Wal97]. Historically speaking, the importance of numerical invariant solutions was recognized through the studies of SSP[Nag90, IT01, KK01].

Using numerical exact solutions

One of the modern tools for estimating the characteristics of non-trivial modes which are expected to govern the turbulent motion and also subcritical transitions is the usage of numerical exact solutions. Here, this tool is based on the conjecture that in phase space "unstable" nonlinear invariant solutions should exist nearby turbulent state[KUvV12]. Actual turbulent motion is considered as an orbit wandering among these invariant solutions. In the following discussion, we assume that $\boldsymbol{X}$ is the element of Hilbert space of a finite dimension, N, corresponding to the size of numerical discretization. Since $\boldsymbol{F}$ in the governing equation (1.5) is continuous, one can expect that the dynamics and the statistical law of the turbulent motion can be described by the approximations obtained with some known solution $\boldsymbol{X}_0$. Usually, $\boldsymbol{X}_0$ is one of the invariant solutions such as stationary or periodic solutions to meet reproducibility. In other words, $\boldsymbol{X}_0$ satisfies the following relation:

$$\boldsymbol{F}'(\boldsymbol{X}_0) \equiv \boldsymbol{F}(\boldsymbol{X}_0) - \boldsymbol{c} \cdot \frac{d\boldsymbol{X}_0}{d\boldsymbol{x}} = 0, \tag{1.17}$$

for a traveling solution with the phase velocity $\boldsymbol{c}$ and for a stationary solution, $c = 0$. Here, $\boldsymbol{x}$ denotes the spatial coordinate.

Let $\boldsymbol{G}(\boldsymbol{X};T) \equiv \boldsymbol{X}(t_0) + \int_{t_0}^{t_0+T} dt\boldsymbol{F}(\boldsymbol{X}(t))$ be the map to the time evolution in T. Then, a certain snapshot $\boldsymbol{X}^0$ of a (relative) periodic solution of the period T is the solution of the following relation:

$$\boldsymbol{G}'(\boldsymbol{X}^0, T, \boldsymbol{x}_0) \equiv \boldsymbol{G}(\boldsymbol{X}^0, T) - \boldsymbol{H}(\boldsymbol{X}^0, \boldsymbol{x}_0) = 0. \tag{1.18}$$

Here, $\boldsymbol{H}(\boldsymbol{X}, \boldsymbol{x})$ denotes the spatial translation: $\boldsymbol{x} \to \boldsymbol{x} + \boldsymbol{x}_0$. Since invariant solutions used for understanding of turbulence motion are unstable, we should directly solve $\boldsymbol{F}' = 0$ or $\boldsymbol{G}' = 0$ generally using the following Newton iteration:

$$\boldsymbol{X}_{n+1} = \boldsymbol{X}_n - (D\boldsymbol{F}'(\boldsymbol{X}_n))^{-1}\boldsymbol{F}'(\boldsymbol{X}_n). \tag{1.19}$$

Here, $(D\boldsymbol{F}'(\boldsymbol{X}))^{-1}$ is the inverse matrix of Jacobian of F' obtained by linearization around $\boldsymbol{X}_0$. This procedure is still heavy computing tasks, because the dimension of $\boldsymbol{X}$ is too high to calculate the inverse matrix which has N^2 components and needs $\mathcal{O}(N^3)$ operations to be solved by the direct method. Thus, an efficient way to get an unstable invariant solution is still an open problem. The details of the numerical methods used in this thesis are explained in Appendix A.

Another way to use numerical invariant solutions is to reproduce an edge state, which is the basin boundary between the laminar state and the turbulent attractor. For subcritical Reynolds number, the flow starting from the laminar state with a small perturbation returns to the laminar state while it goes to turbulence if the amplitude of the perturbation exceeds some threshold. By this method the flow can keep staying on the hypersurface between the laminar state and turbulence: this hypersurface should be identified as the basin boundary in dynamical system's point of view. The previous studies of minimal flow turbulence showed that a simple invariant solution called edge state here, is embedded in the basin boundary and that both stable and unstable manifolds of the edge state give some suggestions about the dynamics of transient behaviors and intermittent bursts[IT01, KKS$^+$16].

Dynamics of localized modes

We now touch on the characteristics of spatially-localized turbulence mentioned above subsection, "(c) Moving of the center of turbulence", in the rest of this subsubsection. As the case of (c), spatially-localized turbulence can be regarded as a moving element with a large internal degree of freedom. The position of spatially-localized turbulence can be important for the

description of its motion when it occupies the approximately constant area. Examples are turbulent puff in pipe flow and typhoon on the earth. When SLTs such as turbulent slugs in pipe flow and turbulent spots in channel flow change their sizes, the velocity of their boundaries, i.e., fronts invading the laminar region is focused on.

The definition of the center of SLT is essentially ambiguous from its turbulent dynamics. However, the prediction and control of the center of SLT is crucial especially for practical reasons. For example, the prediction of the path of a typhoon is one of the main problems on disaster prevention. A detailed discussion on this topic is provided in Chapter 2.

1.1.3 Kolmogorov flow

Solutions of Navier-Stokes equations strongly depend on the way to drive them and also on boundary conditions. However, a precise investigation of models simpler than NS equations plays an important and suggestive role on the understanding of turbulence phenomena. Here, we should adopt a two-dimensional (2D) flow in a periodic box since the 2D system is easy to be treated theoretically and numerically. In incompressible 2D flow, the velocity field denoted by $\boldsymbol{u} = (u_x, u_y)$ can be expressed locally by the stream function denoted by ψ as follows:

$$u_x = \partial_y \psi, \tag{1.20}$$

$$u_y = -\partial_x \psi. \tag{1.21}$$

Note that by using periodic boundary conditions, strong explicit and implicit non-uniformities induced by material walls can be omitted. Navier-Stokes system with the monochromatic force $f = \sin(ny)\hat{\boldsymbol{x}}$ is called Kolmogorov flow.

$$\partial_t \boldsymbol{u} + (\boldsymbol{u} \cdot \boldsymbol{\nabla})\boldsymbol{u} = -\boldsymbol{\nabla} P + \nu \nabla^2 \boldsymbol{u} + \chi \sin(2\pi n y / L_y)\hat{\boldsymbol{x}}, \tag{1.22}$$

$$\boldsymbol{\nabla} \cdot \boldsymbol{u} = 0, \tag{1.23}$$

when χ is the amplitude of the forcing. This system is defined on a periodic domain, $(x, y) \in [0, L_x] \times [0, L_y]$. One must additionally specify the unit flow rate U defined as follows:

$$\boldsymbol{U} = (U_x, U_y) \equiv \frac{1}{L_x L_y} \int_0^{L_x} dx \int_0^{L_y} dy \boldsymbol{u}. \tag{1.24}$$

Considering Galilean transformation $\boldsymbol{u}(x,t) \to \boldsymbol{u}(\boldsymbol{x}\boldsymbol{c}t) + \boldsymbol{c}$ for an arbitrary constant $\boldsymbol{c}$, one can set $U_x = 0$ without loss of generality, and can "NOT" set $U_y = 0$ since the forcing term $\sin(2\pi n y/L_y)\hat{\boldsymbol{x}}$ has the explicit coordinate dependence in y. It is convenient to nondimensionalize and to redefine these governing equations as follows:

$$\partial_t \boldsymbol{u} + (\boldsymbol{u}\cdot\boldsymbol{\nabla})\boldsymbol{u} = -\boldsymbol{\nabla}P + \frac{1}{\mathrm{Re}}\nabla^2\boldsymbol{u} + \sin(ny)\hat{\boldsymbol{x}}, \tag{1.25}$$

$$\boldsymbol{\nabla}\cdot\boldsymbol{u} = 0, \tag{1.26}$$

$$\boldsymbol{U} \equiv \frac{\alpha}{4\pi^2}\int_0^{2\pi/\alpha} dx \int_0^{2\pi} dy \boldsymbol{u}, \tag{1.27}$$

$$(x,y) \in [0, 2\pi/\alpha] \times [0, 2\pi], \tag{1.28}$$

where $(x,y) \in [0, 2\pi/\alpha] \times [0, 2\pi]$. Here, Re is Reynolds number and α is the aspect ratio of the rectangle domain. Thus, the independent control parameters of this model are $(\mathrm{Re}, \alpha, n, U_y)$. This model is originally introduced for studies of instability. In the original setting, n and U_y are set 1 and 0, respectively. From its simplicity, there exist many rigorous theorems for instability such as the existence of bifurcation[AM60, MS61, Iud65, Arn91].

Kolmogorov flow with finite U_y

2D Kolmogorov flow with a finite U_y has plentiful turbulent states[HT15]. Most of the previous studies of Kolmogorov flow deal with a zero unit flow rate system: $\boldsymbol{U} = \boldsymbol{0}$. They clarified that localized dynamics including turbulence can be observed in the wide ($\alpha \ll 1$) system. Note that such localized solutions can be isolated in $|U_y| \neq 0$ system. In this case, several localized solutions can also coexist and interact with each other. Moreover, when $|U_y|$ gets large enough, the flow should decay to the laminar state quickly.

1.1.4 Construction of this thesis

In this thesis, Dynamics and transition in the subcritical regime is considered focusing on spatially-localized turbulence. The subcritical regime is guaranteed by large $|U_y|$ in 2D Kolmogorov flow. The title of Chapter 2 is *Intermittent direction reversals and application of dynamical systems' approach* . In this chapter, we find that there exists a novel localized turbulent state

moving with a constant speed on average and its moving direction changes intermittently. We try to describe its dynamics and the direction change event using dynamical systems' approach. The title of Chapter 3 is *Construction of Navier-Stokes model without material wall to exhibit laminar-turbulence transition as nonequilibrium phase transition*. In this chapter, we construct a simple 2D Kolmogorov flow model to observe subcritical transition belonging to DP universality class.

Chapter 2

Intermittent direction reversals and application of dynamical systems' approach

2.1 Introduction

Spatially-localized turbulent (SLT) states embedded in laminar flows such as puff and stripe, are observed mainly in subcritical transient flows around nonlinear critical Reynolds number both experimentally and numerically[AMdL$^+$11, SMDK14, WPKM08, KKS$^+$16, DSH10, IDT16]. These SLTs play a fundamental role in elucidation of generation, evolution and sustenance of turbulence as well as transition to turbulence.

When considering not globally-occupied but spatially-localized states, motion of turbulent regions should be taken into account. Since turbulence states are localized, the position and velocity of a turbulent state can be defined. Furthermore, these facts may stimulate researchers in more general contexts such as dissipative soliton and self-propelled particles: the former is a moving solitary state in a dissipative system[MD93, CH93, AF00, MD15] and the latter is a simple model of animate lives such as microorganism, bird, fish and their collective motion[VZ12, TIMO14].

In these contexts, a spatially-localized turbulent state can be regarded as a moving element coupled with complex internal freedoms. These moving turbulent regions also are connected with phenomena interfering with our daily life. For example, typhoons, which cause severe disasters, are fully

developed complex turbulence and needless to say, prediction of their paths is still not easy.

The collective behavior of SLTs plays also an essential role in subcritical transitions. In such transient flows, SLTs create their copies and annihilate randomly[AMdL$^+$11]. Recently, experimental and numerical researches in terms of direct numerical simulations (DNSs) and models have uncovered that subcritical transitions in shear flows can be regarded as an absorbing phase transition and its scaling exponents accord with those of directed percolation[ST16, LSA$^+$16a, CTB17a] [1].

To describe the dynamics of complex turbulent states, dynamical systems approach has been widely applied nowadays. In this approach, simple invariant solutions of governing equations such as periodic solutions are adopted as landmarks embedded in a phase space, and a certain realization is identified as a single trajectory visiting these unstable invariant solutions [Nag90, AMRH13, WCA13, KE12, KZE14, ME12, KUvV12, KK01, IT01, CK13, LK14]. Since it is not easy to find unstable solutions based on Newton method for complex flows, several numerical methods have been developed to obtain an initial condition by which Newton iteration converges easily even at relatively higher Reynolds number [TT14, Far16]. These dynamical systems' approach has been extended to the results of laboratory experiments [STGS17]. However, it is a hard task to investigate dynamical properties of spatially-localized states because we must treat a wide range of spatial modes from small ones representing turbulence to large ones isolating turbulence from laminar regions.

While dynamical and statistical properties of flows in relatively small systems at low or moderate Reynolds numbers have been well understood, those of turbulent flows in extended domains at higher Reynolds numbers are not still clarified. This is partially because inhomogeneity induced by walls plays a crucial role in developed wall-bounded flows. In fact, many ingredients of turbulent flows including near-wall dynamics and large scale structures in bulk spontaneously coexist and interact with each other [TI05]. In addition, dynamical description of systems with translational symmetries has been studied for a long time[BBEC15, BCDS15, WCA13]. However, its extension to dynamical systems with huge degrees of freedom such as turbulent flows has just come to be considered recently and is still one of challenging issues[KZE14].

[1] Y.Hiruta, S. Toh, in preparation

As a tractable and simple model representing localized turbulence, we deal with a two-dimensional flow in a doubly-periodic box forced by a single monochromatic external force called Kolmogorov flow. Kolmogorov flow has been widely examined for a longtime to understand mainly mathematical aspects of Navier-Stokes flow such as cascades of supercritical bifurcations to turbulence [GY13, CK13, LK14, LK15, Siv85, Mar87, MS61]. Recently, spatially-localized dynamical states and their dynamical properties have been reported[LK14, LK15]. Solitary spatially-localized turbulent states can exist and even be isolated by introducing the flow rate as a control parameter in the direction in which the Galilean invariance is broken by the forcing[HT15].

In this paper, we investigate novel translational motion of an SLT. In two-dimensional Kolmogorov flow at moderate values of Reynolds number and the flow rate, an SLT shown in FIG.2.1 moves with a nearly constant speed sustaining its direction for a long time and suddenly and intermittently turns around as shown in FIGs.2.2(b) and 2.3(b). Our motivation is to clarify the relationship between this translational motion and the internal dynamics of a single SLT.

The rest of the paper is organized as follows: Sec.2.2 is devoted to the definition and characterization of the flow system. We introduce a co-moving frame to decompose an SLT into its spatial translation and internal dynamics. In sec.2.3, the coarse-grained motion of the center of an SLT is examined. In sec.2.4, we try to describe the motion of the center with representative variables of the internal dynamics of the SLT in the co-moving frame. Concluding remarks are presented in the final section.

2.2 Governing Equation and setting

We focus on two-dimensional (2D) Kolmogorov flow sustained by a steady sinusoidal force. The velocity field $\boldsymbol{u} = (u_x, u_y)$, where the subscripts x and y denote the directions parallel and perpendicular to the force, is governed by the following non-dimensionalised 2D Navier-Stokes equation in doubly periodic domain $(x, y) \in [0, 2\pi/\alpha] \times [0, 2\pi]$:

$$\partial_t \boldsymbol{u} + (\boldsymbol{u} \cdot \boldsymbol{\nabla})\boldsymbol{u} = -\nabla p + \frac{1}{\mathrm{Re}}\nabla^2 \boldsymbol{u} + \sin(ny)\hat{\boldsymbol{x}}, \tag{2.1}$$

$$\boldsymbol{\nabla} \cdot \boldsymbol{u} = 0. \tag{2.2}$$

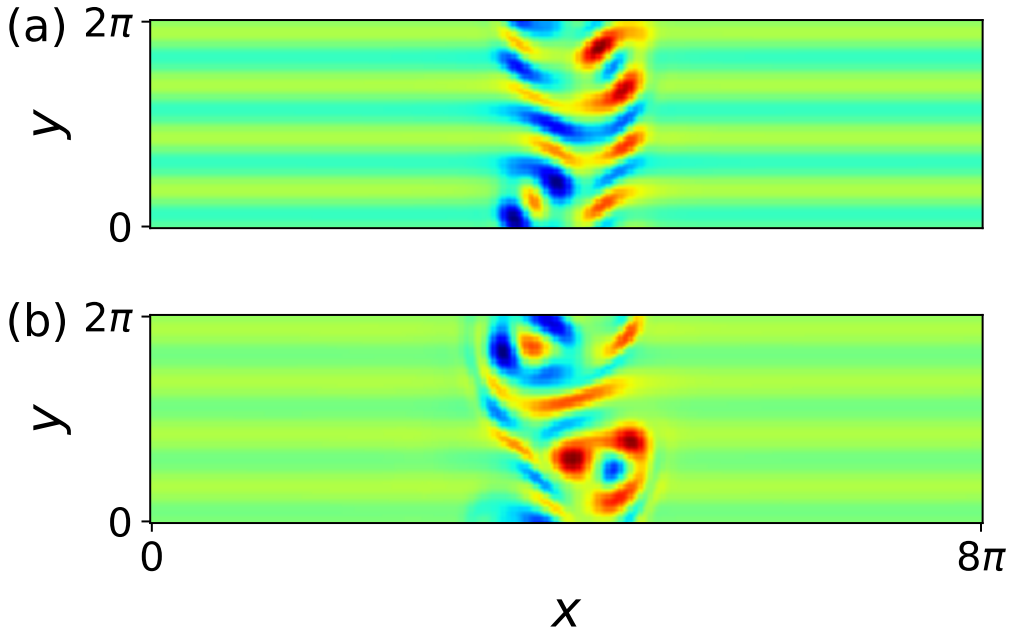

Figure 2.1: Snapshots of vorticity field $\omega(\boldsymbol{x}, t)$ of a moving SLT for $n = 4$ and $\alpha = 0.25$: (a) Re=26.75 and U_y=0.933, (b) Re=50 and U_y=1.46.

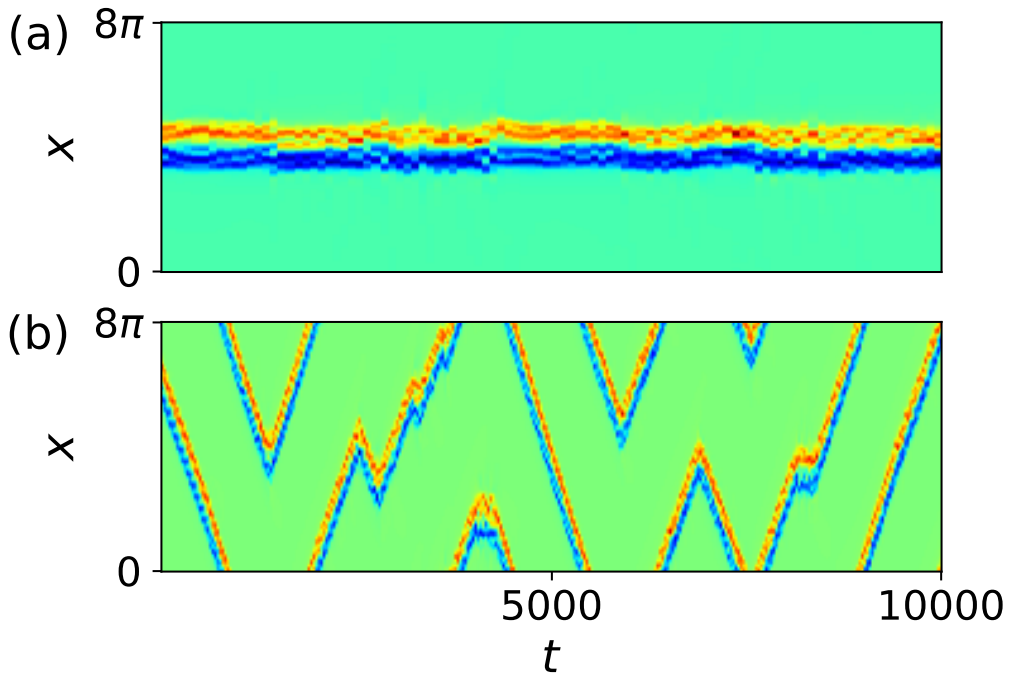

Figure 2.2: Time evolution of vorticity averaged in y-direction $\Omega(x,t)$ for Re=26.75 and $U_y = 0.933$ (a) in the co-moving frame and (b) the laboratory frame.

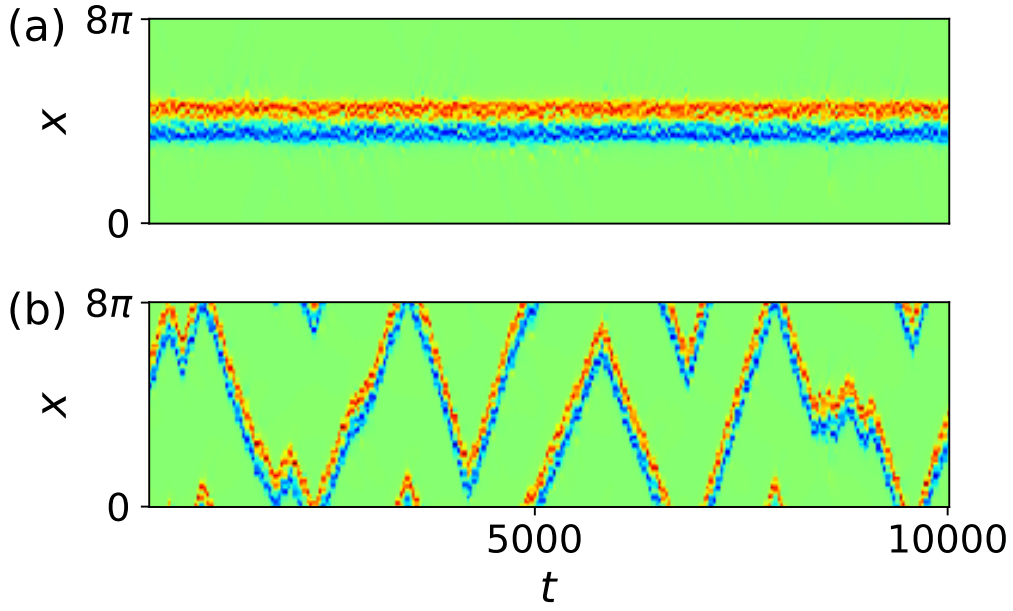

Figure 2.3: The same as FIG.2.2 except for Re=50 and $U_y = 14.6$.

Here, the pressure p is doubly periodic and α, Re, n and $\hat{\boldsymbol{x}}$ denote the aspect ratio of the rectangular domain, Reynolds number, the wave number of the external sinusoidal force and the unit vector in the x-direction, respectively. The average flow rate in y-direction denoted by U_y is a conserved quantity and controls the nature of the flow [HT15]:

$$U_y = \frac{\alpha}{4\pi^2}\int_0^{2\pi/\alpha} dx \int_0^{2\pi} dy u_y = \langle u_y \rangle_{xy}. \tag{2.3}$$

We should note that y-dependence of the forcing breaks Galilean invariance in y-direction. The formulation in Eq.(2.1) for $U_y \neq 0$ is equivalent to one in the reference frame of the zero flow rate with the time-periodical forcing $\sin(n(y - U_y t))\hat{\boldsymbol{x}}$. All variables are non-dimensionalised with length scale $L_y/2\pi$ and timescale $\sqrt{L_y/2\pi\chi}$, where L_y and χ are the hight of the domain and the forcing amplitude. Thus, the characteristic velocity is $\sqrt{L_y\chi/2\pi}$ and Reynolds number is defined as

$$\mathrm{Re} = \frac{\sqrt{\chi}}{\nu}\left(\frac{L_y}{2\pi}\right)^{3/2}. \tag{2.4}$$

Here ν is the kinetic viscosity. Our DNS solves the following equation for the vorticity, $\omega = \partial_x u_y - \partial_y u_x$ with the pseudo-spectral method for spatial discretization using the two-thirds rule for dealiasing and the 2nd order Runge-Kutta (Heun) method for time evolution.

$$\partial_t \omega + (\boldsymbol{u} \cdot \boldsymbol{\nabla})\omega = \frac{1}{\mathrm{Re}} \nabla^2 \omega - n \cos(ny). \tag{2.5}$$

The time and spatial resolutions used for DNSs are 2×10^{-3} and 128 points per 2π, respectively.

This system is equivariant with respect to the action with the following fundamental symmetries:

$$\mathcal{T}_l : \omega(x, y) \to \omega(x + l, y) \quad \left(0 \le l < \frac{2\pi}{\alpha}\right), \tag{2.6}$$

$$\mathcal{S} : \omega(x, y) \to -\omega(-x, y + \frac{\pi}{n}). \tag{2.7}$$

Here, $\mathcal{T}_l$ is a continuous translational symmetry in x-direction, and $\mathcal{S}$ is a discrete shift-and-reflect symmetry which is represented by cyclic group of order $2n$. We also use these two symbols to denote actions on states of a flow as long as there is no misunderstanding.

There are two main control parameters in 2D Kolmogorov flow: Re and the flow rate U_y. Note that for most researches on 2D Kolmogorov flow, U_y is fixed to 0. If U_y is large enough, this system has multi-stable states, one of which is the laminar solution stabilized by the finite flow rate, and others are a single SLT or its coexisting states. For moderate Re and U_y, an SLT moves in a constant speed, including zero, on average and keeps switching its moving direction for suitable values of Re and U_y. Since we are interested in direction reversal events from the point of the relationship between the motion and the internal turbulent dynamics of a single SLT, we limit Re to two values: One is Re = 26.75 and slightly higher Re than the lowest Re, i.e., Re_c at which the reversals of the moving direction starts, and the other is Re = 50 at which the reversal is sustained for a long time and we call this state the reversal state hereafter.

For a single SLT to be sustained in the box, the mean flow rate U_y is set to 0.933 for Re = 26.75 and 1.46 for Re = 50, respectively. For the latter parameter set, the moving direction of an SLT contains quick fluctuations as well as relatively slow and intermittent switching. The other system parameters, n and α are fixed to $(n, \alpha) = (4, 0.25)$ in this paper.

In the lower Re case, the initial condition assigned is an unstable relative periodic solution (URO), which is a time-periodic solution with a spatial shift. The URO is a continuation solution of the stable solitary relative periodic solution obtained in Ref.[HT15]. By the symmetry $\mathcal{S}$, this URO can have both positive and negative velocities, $c_{\mathrm{URO}} = \pm 0.02$, in x. The period of the URO is ~ 60 and characterizes the time scale of the internal turbulent fluctuation.

Because of numerical errors in the initial condition, this solution falls into an SLT in a few periods and gets to switch intermittently its moving direction. Furthermore, around at $t \sim 10^5$ it suddenly ceases to move with a constant speed even on average and begins to hang around changing its moving direction quickly as shown in FIG.2.4. This transient suggests that there exist several different types of SLT states: A kind of transition from traveling to standing SLT. However, we focus on the first (traveling) SLT state observed before the second transition.

For Re = 50 and U_y=1.46, we fail to obtain a URO solution for an initial condition. However, based on numerical observations that the state of flow has a tendency to fall into a unique state similar to the transient reversal state at Re = 26.75, we picked this transient reversal state as an initial condition to investigate the reversal state. The reversal states obtained with several initial conditions are sustained for a long time at least $t \sim \mathcal{O}(10^6)$.

We introduce a frame system to separate the motion from the internal turbulent dynamics of each SLT. Here the motion of an SLT stands for the evolution in a coarse-grained time of a point representing the location of the SLT. We call this point the center of the SLT. An SLT travels both in x and y directions. The translation in y is mainly caused by the mean vortex pair which forms a kind of a Karman vortex street traveling with a constant speed on average while the translation in x is caused by both the coarse-grained vortical structure and the short time internal turbulent dynamics. Therefore we give our attention to the motion in x of an SLT.

This frame system is an extension of Galilean transformation and is defined by formally applying a time-dependent translational symmetry:

$$\hat{\omega}(x, y, t) = \mathcal{T}_{l(t)}\omega(x, y, t) = \omega(x + l(t), y, t), \tag{2.8}$$

where $l(t)$ is a time dependent shift in x-direction. We call the case of $l(t) = 0$ the laboratory frame and the case of $l(t) = -X(t)$ the co-moving frame where $X(t)$ is an approximate or coarse-grained location of the SLT but

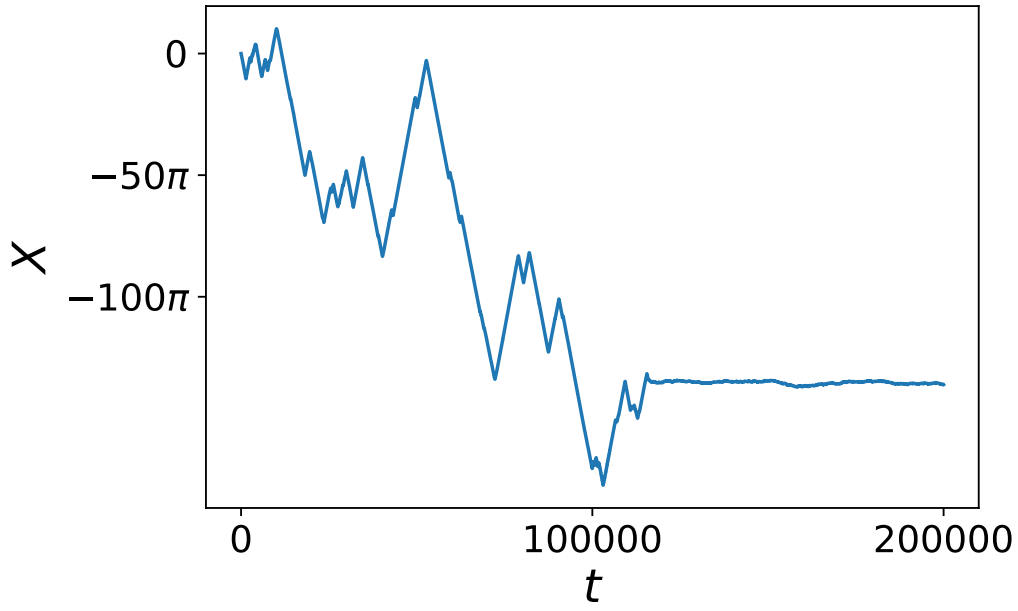

Figure 2.4: Long time evolution of the center ,$X(t)$, of the SLT shown in FIG.2.2 for Re=26.75 and $U_y = 0.933$. The SLT transits from a moving state to a standing state at $t \sim 120000$.

its definition includes some ambiguity originated from the internal turbulent fluctuation. We define $X(t)$ by setting the phase of the first Fourier mode of the vorticity field with $k_x = \alpha$ and $k_y = 0$ to $\pi/2$. Hereafter, we call $X(t)$ the center of the SLT. Note that if the velocity of the center of the SLT, i.e., $V(t) = dX(t)/dt$ is not a constant, the dynamics of the SLT even in the co-moving frame is coupled with the motion of the SLT.

Moreover, we expect (not guaranteed) that the center of the following average vorticity $\Omega(x,t)$ stays around the same positions in the co-moving frame:

$$\Omega(x,t) = \frac{1}{2\pi}\int_0^{2\pi} dy\omega(\boldsymbol{x},t). \tag{2.9}$$

This method has been adopted for one-dimensional PDE and three-dimensional turbulent pipe [BBEC15, BCDS15, WSC16]. Both in the laboratory and co-moving frames, the time evolution of $\Omega(x,t)$ is shown in FIG.2.2 and FIG.2.3.

In the laboratory frame, sudden and intermittent changes of the moving direction of the SLT can be observed. In the co-moving frame, the SLT stands around the same position in time with small fluctuations. This enable us to make a decomposition into the motion of the SLT, i.e., $X(t)$ and the internal turbulent dynamics, $\hat{\omega}(\boldsymbol{x},t)$ defined in (2.8).

2.3 Motion of moving turbulence

We focus on the nature of the switching of the moving direction. Because even the coarse-grained center of an SLT, $X(t)$, still fluctuates in a time scale of the order of the internal dynamics of the SLT, the intervals between adjacent reverses of the moving direction denoted by Δt, i.e., the residence time are evaluated with a velocity averaged over an interval T defined as

$$\overline{c}_T(t) = \frac{1}{T}\int_t^{t+T} dt' \frac{dX}{dt'}(t') = \frac{X(T+t)-X(t)}{T}. \tag{2.10}$$

The center of an SLT does not move in one-direction in short time scale even if an SLT moves in the same direction in the coarse-grained scale because the average vorticity Ω stays around the same position but strongly fluctuates in the translational direction especially in the higher Re case as shown in FIG.2.2 and FIG.2.3. To detect the direction reversal in a coarse-grained time, we set $T = 100$, which is longer than the typical time scale of the

internal turbulence dynamics. This typical time scale is ~ 60 and of the order of the period of the URO adopted as the initial condition. The subscript T is omitted hereafter for simplicity.

The evolutions of the center $X(t)$ and the average velocity $\overline{c}(t)$ are shown in FIG.2.5. The average velocity $\overline{c}(t)$ takes roughly two values, i.e. $\pm|c_{\max}|$ and a direction reversal occurs when $\overline{c}(t)$ crosses zero. In this sense, the average velocity $\overline{c}(t)$ is an adequate variable to detect direction reversals. This also suggests that at least there are two (that is, twin) unstable invariant sets with $\pm|c_{\max}|$ about one of which the SLT wanders and the direction reversal corresponds to switching between the stays around these sets. We expect that these invariant sets are close to the twin URO one of which is adopted as the initial condition.

In the higher Re case, the histogram of the number of the residence time Δt larger than t denoted by $F(\Delta t > t)$ is shown in FIG.2.6 and the exponential decay is suggested. Note that the average residence time estimated with the decay rate of the exponential decay is $\tau \sim 700$ and sufficiently longer than both the average time $T = 100$ and the period of the URO, about 60 in the normalized time unit.

The exponential-decay tendency observed in $F(\Delta t > t)$ reminds us of a random telegraph signal which is produced by the Poisson process[AVOS03, VEE$^+$17]. This suggests that the aforementioned twin invariant sets corresponding to SLTs with the positive and negative velocities in x have complicated structures different from simple spiral chaos such as Lorenz attractor which has a characteristic time scale corresponding to the period of the rotation of the spiral motion and thus the residence time is roughly integral multiple of the characteristic time. This, however, depends strongly on the coarse-grained time scale. As shown in FIGs.2.5 and 2.7, coarse-grained scale switchings occur in a few steps, and thus this phenomenon could be of large scales and affected by smaller scales that may belong to the internal turbulence and be regarded as a kind of noise, though the mechanism of the switching has not been understood, yet. Anyway, we should carefully select a well-acted projection to describe the trajectory in a phase space.

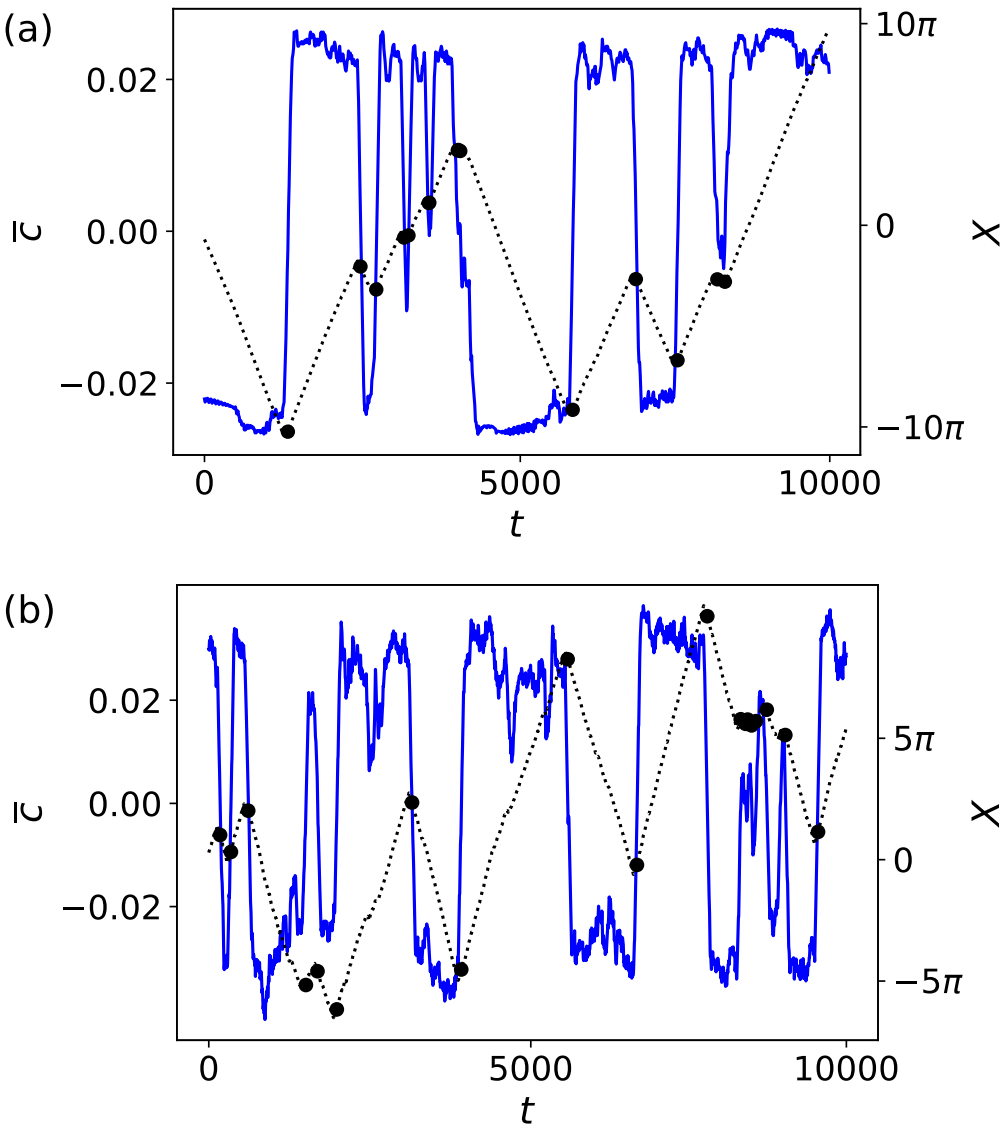

Figure 2.5: Time evolutions of the average velocity $\bar{c}$ (blue solid line) and the central position of SLT X (black dotted line). Large black dots denote direction reversals at (a) Re=26.5 and (b) Re=50.

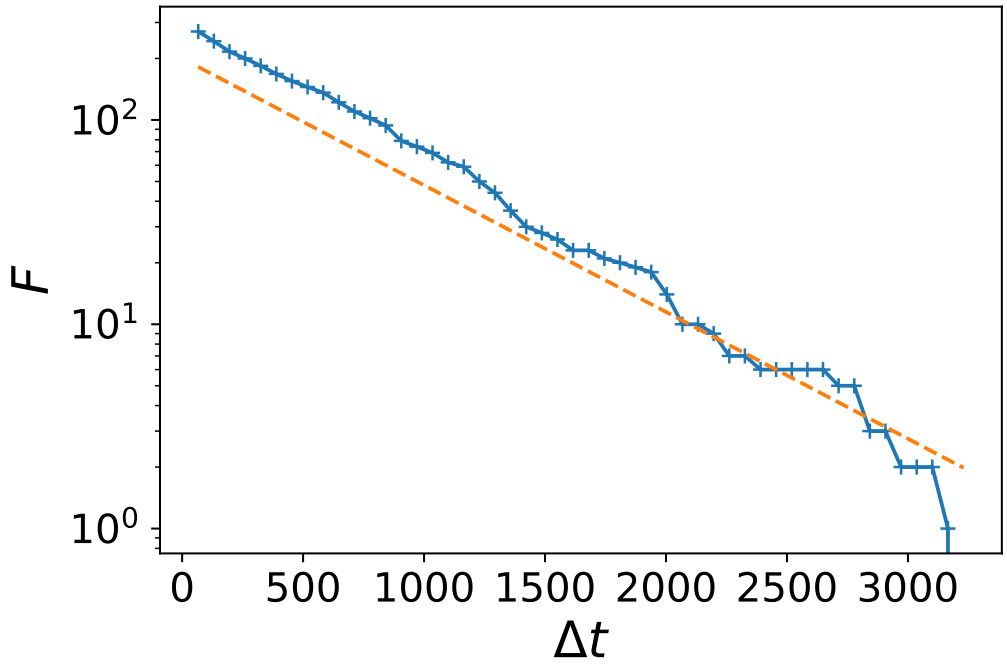

Figure 2.6: $F(\Delta t)$ for (Re, U_y)=(50,1.46). Dashed straight line is $F = 2 \times 10^2 \exp(-\Delta t/700)$ for guide.

2.4 Relation between moving direction and internal turbulent dynamics

In this section, we try to describe the motion of a single SLT in the phase space in relation to internal turbulent dynamics especially in terms of the symmetry focusing on the correlations between the traveling direction and variables in the co-moving frame. In the lower Re case, to clarify the role of the twin URO we will draw a phase portrait based on the standard method used especially for minimal wall bounded flow[GHC08].

To begin with, we introduce some coarse-grained variables that characterize the asymmetric nature in x of the internal turbulent dynamics observed in the co-moving frame based on $\mathcal{S}$ which allows an SLT to travel both to the negative and positive directions in x. The first one is the following quantity evaluated simply by the maximum and minimum values of vorticity:

$$s(t) = \max_{\boldsymbol{x}} \omega(\boldsymbol{x}, t) - |\min_{\boldsymbol{x}} \omega(\boldsymbol{x}, t)|. \tag{2.11}$$

Since the transformation $\mathcal{S}$, $x \to -x$ and $y \to y + \pi/n$, changes the sign of the vorticity $\omega(\boldsymbol{x}, t)$, the sign of $s(t)$ also changes as follows:

$$\mathcal{S}s(t) = -(\min_{\boldsymbol{x}} \omega(\boldsymbol{x}, t)) - |-\max_{\boldsymbol{x}} \omega(\boldsymbol{x}, t)| = -s(t). \tag{2.12}$$

The variable $s(t)$ evaluates the degree of the asymmetry of the vorticity distribution of an SLT. This asymmetry is the origin of the asymmetry of $s(t)$ and thus closely related to the direction reversal.

Since the maximum and minimum of $\omega(\boldsymbol{x}, t)$ fluctuate quickly in time, the average or coarse-grained $\overline{s}$ should be also introduced:

$$\overline{s}_T = \frac{1}{T} \int_t^{t+T} dt' s(t). \tag{2.13}$$

The subscript T of $\overline{s}_T$ is omitted hereafter for simplicity. As shown in FIG.2.8, $\overline{s}$ correlates adequately with the moving direction of an SLT in the two Re cases. However, they fluctuate more strongly than $c_T(t)$ and this tendency is enhanced in the higher Re case. This suggests that the internal turbulence correlates the motion of a single SLT, but the correlation between $\overline{s}_T(t)$ and $\overline{c}_T(t)$ is not sufficient enough for $\overline{s}_T$ to be used for deterministic and quantitative description of the motion of the SLT.

We next introduce another variable representing a distance from these invariant sets more quantitatively. The vorticity field in the co-moving frame $\hat{\omega}(\boldsymbol{x}, t)$ is projected onto the two fields defined by the average under the condition that the traveling direction is positive or negative, respectively. The negative mean state ϕ_n and the positive mean state ϕ_p are defined numerically as follows:

$$\phi_n(\boldsymbol{x}, t) = \langle \hat{\omega}(\boldsymbol{x}, t) \rangle_{\overline{c}(\hat{\omega})<0}, \tag{2.14}$$

$$\phi_p(\boldsymbol{x}, t) = \langle \hat{\omega}(\boldsymbol{x}, t) \rangle_{\overline{c}(\hat{\omega})>0}, \tag{2.15}$$

$$\tag{2.16}$$

where the bracket $\langle\ \rangle$ and its subscript denote an ensemble average in the co-moving frame and the condition under which the average is calculated, respectively. These two fields are expected to approximate the twin invariant sets.

The projections onto ϕ_n and ϕ_p are carried out with the internal product $\langle \phi | \omega \rangle$ between real functions as follows:

$$a_n(\hat{\omega}) = \frac{\langle \phi_n | \hat{\omega} \rangle}{||\hat{\omega}||^2}, \tag{2.17}$$

$$a_p(\hat{\omega}) = \frac{\langle \phi_p | \hat{\omega} \rangle}{||\hat{\omega}||^2}, \tag{2.18}$$

$$\langle f | g \rangle = \frac{\alpha}{4\pi^2} \int dx dy f(x, y) g(x, y), \tag{2.19}$$

$$||f|| = \sqrt{\langle f | f \rangle}. \tag{2.20}$$

The difference between the coefficients denoted by $a(t) = a_p(\hat{\omega(t)}) - a_n(\hat{\omega(t)})$ also evaluates the asymmetry of an SLT and is expected to indicate the direction of the motion, because the moving direction of the URO is determined by the asymmetry of the vorticity field and an SLT seems to stay around one of the invariant sets close to the corresponding URO. To clarify the importance of the URO, we draw a phase portrait in the 2D space spanned by $\overline{c}$ and a using the strobe map in the lower Re case as shown in FIG.2.7. Most points are concentrated in the two separated sets and the twin URO are embedded in these sets where a reversal event is identified as a transient path connecting the two separated sets. As shown in FIG.2.8, $a(t)$ reproduces roughly the switching process as the $\overline{s}(t)$. However, in the higher Re

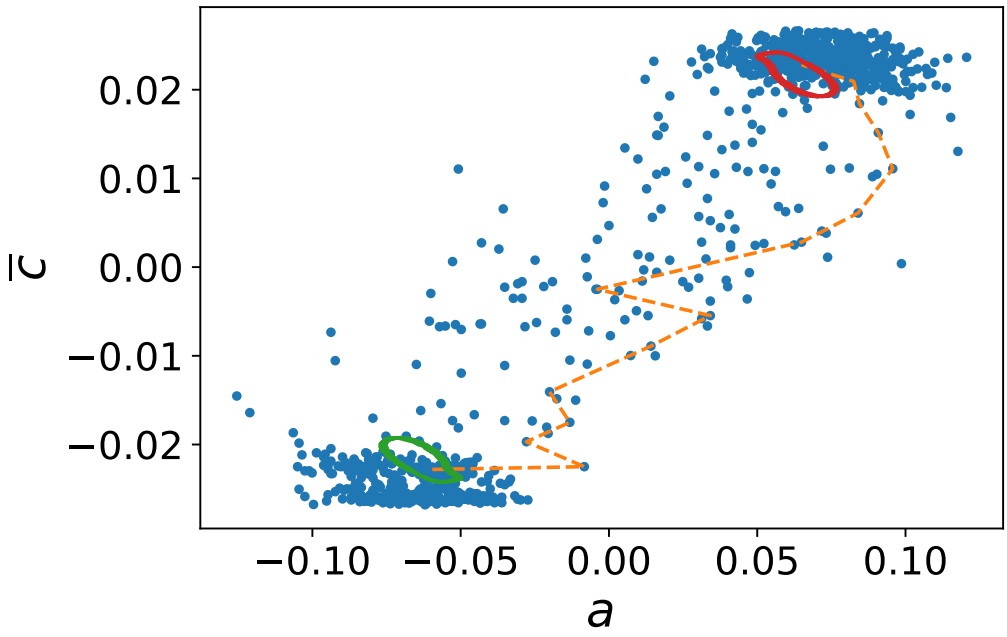

Figure 2.7: Phase portrait for Re= 26.75 and $U_y = 0.933$. Dots indicate the strobe map with interval 10 non-dimensionalised times. Hashed line indicates a reversal around t∼1000 in FIG.2.5. Closed loops indicate the twin URO. One of the twin URO is used as the initial condition, and the other is just the symmetrical one (also a solution of NS equation.)

case, both the two quantities, $\overline{s}(t)$ and $a(t)$, which are coarse-grained representatives of the internal turbulent dynamics, tend to be less able to follow the average velocity $\overline{c}(t)$, although the two moving states with the velocities $\sim \pm|c_{\max}|$ and the direction reversal are still clearly identified. This suggests that even though the twin or multiple invariant sets are still discriminated clearly by the moving direction, the number of variables or the dimension of the phase space required to describe the internal turbulent dynamics which is directly related to the coarse-grained motion of an SLT seems to increase with Re.

This difficulty is inherited by their higher order moments. To see this, we define the dispersion, the second moment of the fluctuations of the vorticity

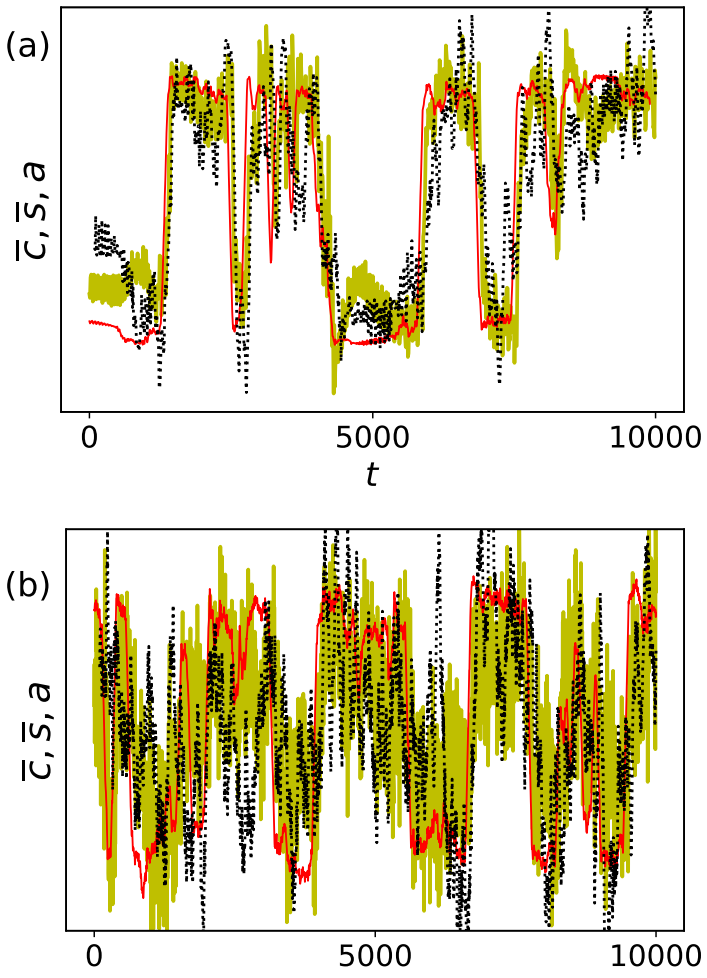

Figure 2.8: Time evolutions of $\overline{c}$ (red thin solid line), $\overline{s}$ (black dotted line) and $a = a_p - a_n$ (yellow thick solid line):(a) for Re=26.75 and $U_y = 0.933$ and (b) for Re $= 50$ and $U_y = 1.4$. Minimum and maximum values are (a) (-0.125,0.126) for a, (-0.0268 0.0266) for $\overline{c}$, (-1.36 1.79) for $\overline{s}$ and (b) (-0.0371 0.0351) for a, (-0.0174 0.0157) for $\overline{c}$, (-1.50 1.36) for $\overline{s}$.

field under the condition $\overline{c} < 0$ as follows:

$$\delta\Omega_n^2(x) = \int_0^{2\pi} dy \delta\omega_n^2(x,y), \tag{2.21}$$

$$\delta\omega_n^2(x,y) = \langle\omega^2(x,y)\rangle_{\overline{c}<0} - \langle\omega(x,y)\rangle_{\overline{c}<0}^2. \tag{2.22}$$

Figure 2.9 shows the dispersion $\delta\Omega_n^2(x)$ in both Re cases and is compared with that of the URO. Since the SLT travels to the left, i.e., $\overline{c} < 0$, the fluctuation on the left side or the front of the SLT is stronger than that of the right side or the back front, while the absolute value of the average vorticity is larger on the back front than on the front. As shown in FIG.2.9, this characteristics of the vorticity fluctuation is shared with a left traveling URO of $c_{\rm URO} = -0.02$ which is a periodic solution in the co-moving frame though the asymmetry of the dispersion of the URO is weaker than that of the SLT. This also supports the simplified picture of the phase space constituted by several twin unstable invariant sets each of which might correspond to a one-way traveling SLT. The asymmetry of the vorticity fluctuation is observed in other traveling localized states or invasion-fronts of turbulence.[BSM$^+$15, TT16] In the higher Re case, the asymmetry of vorticity fluctuation is weaker than that in the lower Re case. Therefore we need variables more susceptible to geometrical or temporal characteristics of the SLT to resolve the internal turbulent dynamics.

2.5 Concluding remarks

We have found that a single spatially-localized turbulence (SLT) exists stably and travels in x switching the moving direction randomly and intermittently. By introducing the coarse-grained center $X(t)$ and traveling velocity $\overline{c}_T(t)$ of the SLT, we have characterized the traveling motion and these switching events in the coarse-grained time scale. Even in the relatively high Re case, $\overline{c}_T(t)$ takes roughly two values $\pm|c_{\rm max}|$ and the residence time Δt is thought to obey the exponential distribution, which suggests that $\overline{c}_T(t)$ can be approximated by a random telegraph signal. At least (several) twin attracting invariant sets, each of which corresponds to a one-way traveling SLT and may be close to unstable relative periodic solutions (URO), are embedded in the attractor of the moving turbulence. Since we expect that like a self-propelled particle the motion of a single SLT is controlled by the characteristics of the internal turbulence, the time evolution of the flow is decomposed into the

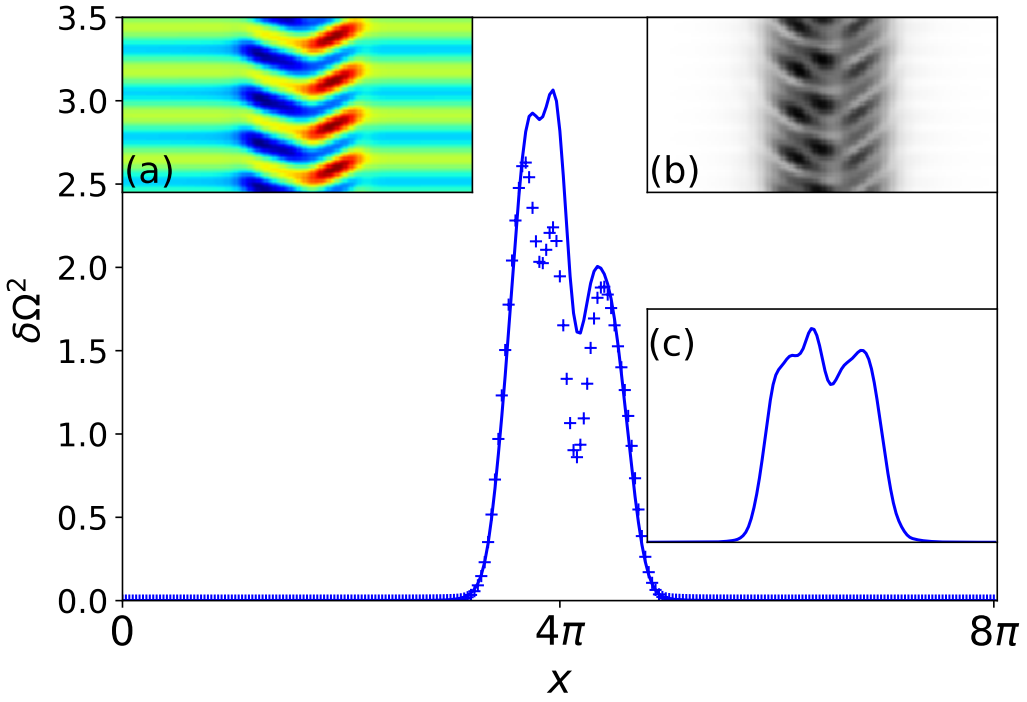

Figure 2.9: Dispersion of vorticity field $\delta\Omega_n^2(x)$ defined in Eq.(2.21) for Re=26.75 and U_y=0.933. The average is taken under the condition $\bar{c} < 0$: Solid line for DNS and plus signs for URO. Inset(a) shows a mean vorticity field $< \omega >_{\bar{c}<0}$ and inset(b) shows dispersion field $\delta\omega_n^2(x, y)$. Inset(c) shows $\delta\Omega_n^2(x)$ for Re=50 and U_y=1.46. Each inset shows only a main part of the field.

coarse-grained motion of the center of the SLT and the accompanying turbulent field by defining the co-moving frame with $X(t)$. We have introduced two coarse-grained variables $\overline{s}_T(t)$ and $a(t)$ characterizing the asymmetry in x of the internal turbulence: $\overline{s}_T(t)$ simply estimates the asymmetry of the vorticity distribution of the SLT and $a(t)$ represents the difference between the approximated distances from the twin unstable sets one of which is projected onto the other by the discrete shift-and-reflect symmetry $\mathcal{S}$.

Reversal detection using symmetry-related variable $\overline{s}(t)$ loses reliability in the higher Re case although the moving direction can be determined well. This fact means that the asymmetry of a traveling solution made by symmetry-breaking is masked by turbulent dynamics. Focusing on the coarse-grained motion and regarding internal turbulent fluctuation as a noise, it is easy to make a Langevin model which can reproduce the stochastic nature of the switching events. However, such a model has not been derived from the governing equation yet. We have tried to study the switching process rather in a topological way focusing on a global structure of the phase space.

Invariant solutions should play a key role in more reliable description of moving turbulence at higher Re. It is expected that a fixed point like URO embedded in each of the twin, i.e., a pair of chaotic attracting sets mimics the average quantity for each direction as suggested by FIG.2.9. These invariant solutions also will help us to attain more quantitative and precise understanding of SLTs.

This type of intermittent switching can be observed in other flows: reversal of Large Scale Circulation in a steady forced flow [Som86, MHFV15] and thermal driven flow[SNS$^+$10, NHX15]. Reversals of flow field can also be observed in minimal channel flow[NDL17]. The approach based on a low dimensional model derived by Galerkin method is useful to study such a transition[SFB16]. We expect that by this approach with the invariant solutions mathematical models representing a moving SLT can be developed.

It is interesting and important to study states consisting of a number of SLTs[HT15]. Such a multiple SLT state in Kolmogorov flow also can contribute as one of the most simple and tractable examples in the elucidation of turbulence transitions observed in wall-bounded flows. However, our approach introduced in this paper needs some improvements in the definitions of the coarse-grained quantities such as positions, velocities and ones representing internal turbulent dynamics.

Concerning subcritical turbulence transition as non-equilibrium phase

transition, where SLTs play a key role, "moving" SLTs that are observed there may affect the determination of critical exponents and/or even a class of the transition itself. In fact, to do so spatial and temporal intervals of laminar regions have been utilized, but fast moving SLTs might modify the distribution of such intervals which blurs the estimation of critical exponents. At least, the correlation length between SLTs can be much longer than the length scale of the support of an SLT. This can be suggested from the relationship between lattice model(XY model) and self propelled particle model(Vicsek model)[MW66, VCBJ$^+$95, TT95, VZ12].

Chapter 3

Construction of Navier-Stokes model without material wall to exhibit laminar-turbulence transition as nonequilibrium phase transition

3.1 Introduction

Turbulence, macroscopically complex behavior, is seen in a wide range of phenomena in nature not only on a scale of our daily life such as the stream-flow of a river and experiments in laboratory[Rey83, Col65] but also from quantum turbulence of superfluid[KT05, TFY17] to cosmic scales[BR11]. It can be regarded as a class of solutions of hydrodynamic equations whose energy is distributed into a wide range of scales. However, we have not completely uncovered the sustaining mechanism of turbulence even for the flow in a circular pipe driven by the pressure gradient[Rey83, ESHW07, WPKM08].

Then, the problem of turbulence transition is crucial not only out of scientific interest but also engineering or practical needs of flow control. Recently, turbulence transition has been approached from the view of statistical physics. Unlike supercritical transition where a fixed point corresponding to the laminar state becomes linearly unstable[Lan44, Hop48, Lor63, RT71], the subcritical transition is difficult to be dealt with since dominant modes

are unclear because of nonlinearity, complexity, and locality. In subcritical regimes of canonical wall-bounded flows, nonlinear spatially-localized turbulent states (SLTs), such as a turbulent puff in pipe flow, is often observed, and they seem to expand or decay locally and randomly[AMdL$^+$11].

Such local and random behaviors of agents of turbulence recall nonequilibrium phase transition via spatiotemporal intermittency with an absorbing state, which corresponds to a stable laminar state, and the most fundamental universality class here is a directed percolation (DP) universality class[Pom86, CM88, Hin00]. The DP universality class is supposed to appear under simple conjectures such as locality and stochastic behaviors of dynamics[Hin00]. Thus, DP can be seen in a wide range of models such as epidemics and synchronizations. We can expect that various flows share a universal spatiotemporal characteristic around critical Reynolds number. By laboratory experiments and simulations of Navier-Stokes model flows[LSA$^+$16b, ST16, CTB17b] it is confirmed that the critical exponents for turbulence fraction and spatiotemporal structures are satisfactorily consistent with those of the DP universality class.

Recent developments of understanding of small systems and SLTs assist us to identify the unit of turbulence and its dynamics [Nag90, Jim90, Wal97, AMRH13, WCA13, KE12, ME12, KK01, IT01, KUvV12, GHC08]. Based on such ideas, several phenomenological models in terms of SLTs were submitted to describe statistics of near-wall flows[Bar11, AE12, Bar16, SHG16] and some of them successfully reproduced not only puff but also slug states and their expanding speeds[BSM$^+$15].

However, from the point of view of the governing equations, which are nonlinear partial differential equations with global couplings, the dynamics of fluid should strongly depend on the way to be driven and boundary conditions as well as spatial dimension. Local dynamics in incompressible flows is affected by long-range interactions due to the pressure gradient term, while the pressure also contributes to local dynamics itself. Thus, the mechanism of sustenance of SLT and the locality of its dynamics are not obvious and remain open problems[KUvV12].

One of the main motivations of this work is to examine the generality of transitions via spatiotemporal intermittency. While stochastic or deterministic models exhibiting the DP universality class transition have a lot of examples and long history, corresponding laboratory experiments conducted so far are not enough. Among them, the first clear one[TKCS07, TKCS09] was done only in recent years. The mechanism and conditions for the DP

transition to be realized in the real world are still unclear. In this sense, further examples of the DP transition especially related to hydrodynamics are still in demand.

We seek candidates in two-dimensional (2D) Navier-Stokes models in the following three reasons. The first is that we should search for a new model not resembling to wall-bounded flows from our aim of generality. The second is to confirm the effects of the pressure gradient on the DP universality. We should note that 2D flows can have some disadvantages for the locality of the dynamics governing the DP, since the strength of the interaction through the pressure gradient in general seems to be a fatter tail, $\sim |r|^{-1}$, than that of 3D flows, $|r|^{-2}$. In this sense, the 2D flows are in the most severe situation among Navier-Stokes models in terms of the locality of the dynamics. If any 2D models exist, we expect that DP or DP-like transitions can occur in a relatively wider class of Navier-Stokes systems except for wall-bounded flows and related models. As the third reason, in general, flows with material wall boundaries in a sufficiently huge box are difficult to be dealt with directly using the Navier-stokes equations since the walls induce both explicit and implicit inhomogeneities in the flows. This difficulty prevents us from relating large scale behaviors of turbulence such as subcritical transitions to relatively well-known dynamics of small systems[Nag90, Jim90, Wal97, AMRH13, WCA13, KE12, ME12, KK01, IT01, KUvV12, GHC08]. Thus, a tractable model free from walls is also desired to investigate the generality of subcritical transitions of the Navier-Stokes systems.

One of the most simple 2D flows sustaining turbulence called Kolmogorov flow (KF) was submitted to investigate routes to turbulence[AM60, MS61, Siv85, GYM83, Yam86, Mar87]. Kolmogorov flow has been employed to investigate in details the characteristics of solutions of the Navier-Stokes equations and also as a test field for novel ideas of complex solutions[GY13, CK13, Far16, LK15]. Recently, solutions in which spatially-localized chaotic regions and steady regions coexist were found even in 2D Kolmogorov flow (2DKF)[LK14, HT15, HT17].

In this paper, we report observations of a subcritical laminar-turbulence transition belonging to the DP universality class in a pure 2D flow as shown in FIG.3.1. We also discuss the origin of the linear stability of the laminar solution, the locality of the dynamics and the conditions for the DP class transition to be realized in this 2D Navier-Stokes model.

The rest paper is organized as follows: Sec 3.2 is devoted to the definition of the flow system. In Sec.3.3, we estimate the flow state numerically and

theoretically. Critical Re of the laminar state is estimated there. In Sec.3.4, quenching experiments are conducted from high Re to target Re. It is shown that the scaling of turbulence fraction and histograms of the laminar gaps are consistent with those of DP universality class. Sec.3.5 is concluding remarks.

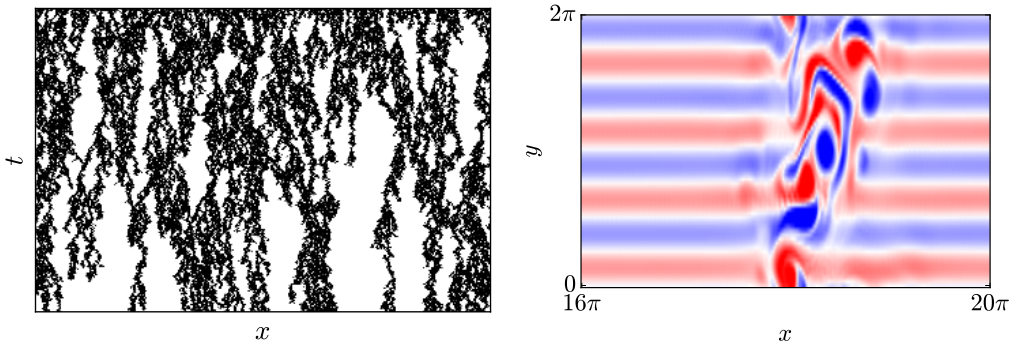

Figure 3.1: Visualization of the flow for (Re ,Reγ, U_y, n, α) = (242, 30, 0.5, 4, 1/256). (a) Typical time evolution of turbulent region(black). White region denotes laminar region. (b) Snapshot of a part of the whole domain, $x \in [16\pi, 20\pi]$, using vorticity ω. The whole domain is $x \in [0, 512\pi]$.

3.2 Governing equation and setting

We focus on the 2D Kolmogorov flow (2DKF) with the linear drag force in a doubly periodic box $(x, y) \in [0, 2\pi/\alpha] \times [0, 2\pi]$. The velocity field $\boldsymbol{u} = (u_x, u_y)$ is governed by the 2D Navier-Stokes equation with a steady sinusoidal force in non-dimensionalized form as follows:

$$\begin{aligned} \partial_t \boldsymbol{u} + \boldsymbol{u} \cdot \boldsymbol{\nabla} \boldsymbol{u} &= -\boldsymbol{\nabla} P - \gamma(\boldsymbol{u} - U_y \hat{\boldsymbol{y}}) \\ &\quad + \frac{1}{\mathrm{Re}} \nabla^2 \boldsymbol{u} + \sin(ny)\hat{\boldsymbol{x}}, \qquad (3.1) \\ \boldsymbol{\nabla} \cdot \boldsymbol{u} &= 0, \qquad (3.2) \end{aligned}$$

where α, Re, γ, n, $\hat{\boldsymbol{x}}$ and $\hat{\boldsymbol{y}}$ denote the aspect ratio of the rectangle domain, Reynolds number, the coefficient of drag force, the wave number of the external force, the unit vectors in x and y, respectively. The pressure function

P is doubly periodic. The velocity averaged over the box and the unit flow rate in y-direction are denoted by $\boldsymbol{U}$ and U_y which are defined as follows:

$$\boldsymbol{U} = \frac{\alpha}{4\pi^2}\int dxdy\boldsymbol{u} = (0, U_y). \tag{3.3}$$

Note that since the y dependence of the external force breaks Galilean invariance in y, the unit flow rate U_y is a control parameter of the system. To non-dimensionalize the governing equation we use $L_y/2\pi$ for the characteristic length scale where L_y is the length of the box in y-direction in the dimensional system. For the work rate of the force to be $\mathcal{O}(1)$, the characteristic time is set to $\sqrt{L_y/2\pi\chi}$ where χ is the amplitude of the sinusoidal force. The linear drag force is typically originated from weak but inevitable effects of material walls[STM$^+$14, STGS17]. For the scales longer than the nondimensional length $L_{\rm drg} \sim (\gamma{\rm Re})^{-1/2}$, the drag term dominates the viscous term in Eq.(3.1). We expect that the drag force decays large scale structures of the system size formed by the energy transfer toward large scales as occurring in 2D inverse-cascade turbulence[Kra67, KM80, LBF$^+$14].

Our direct numerical simulation (DNS) solves the governing equation for the vorticity $\omega = \partial_y u_x - \partial_x u_y$ with the pseudo-spectral method for spatial discretization using the two-thirds rule for de-aliasing and the 2nd order Runge-Kutta (Heun) method for time evolution. The time and spatial resolutions used for DNS are 2×10^{-3} and 64 points per 2π, respectively.

3.3 Parameter dependence of flow state

3.3.1 Stability of the laminar solution

When a subcritical laminar-turbulence transition is realized in 2DKF, the laminar state should be linearly stable at least. First, we check the stability of the following laminar state which is the stationary solution with global x-translational symmetry and denoted by $\boldsymbol{u}_{\rm lam}(U_y)$:

$$\boldsymbol{u}_{\rm lam}(U_y) = \frac{\rm Re}{D}\sin(ny+\theta)\hat{\boldsymbol{x}} + U_y\hat{\boldsymbol{y}}. \tag{3.4}$$

Here, $\tan\theta = -{\rm Re}U_y n/(n^2+\gamma{\rm Re})$ and $D^2 = (n^2+\gamma{\rm Re})^2 + (n{\rm Re}U_y)^2$. This one-parameter form of Eq.(3.4) can be applied approximately for a part of the whole system and this locally-embedded laminar profile can take a certain

value of the local unit flow rate, i.e., β which is not necessarily equal to the unit flow rate U_y. Hereafter, we call $\boldsymbol{u}_{\rm lam}(U_y)$ as the global laminar (GL) state and $\boldsymbol{u}_{\rm lam}(\beta)$ as a local laminar state, respectively.

For $\gamma = 0$, we can estimate the critical Reynolds number, $\mathrm{Re_l}$, for the linearly unstable GL state under the assumption that the GL state is unstable for a long-wave disturbance in x-direction.

The vorticity equation for $\gamma = 0$ is rewritten in terms of the doubly periodic stream function Ψ as follows:

$$\partial_t \nabla^2 \Psi - \{\Psi, \nabla^2 \Psi\}_{xy} + U_y \partial_y \nabla^2 \Psi - \frac{1}{\mathrm{Re}} (\nabla^2)^2 \Psi = n \cos(ny), \tag{3.5}$$

where $\{f, g\}_{xy} = \partial_x f \partial_y g - \partial_y f \partial_x g$.

We search a stationary solution that is the GL state with small long-wave modes by the perturbation expansion:

$$\Psi(x, y) = \Psi_{\rm lam}(y) + \sum_{i=0} \epsilon^i \Psi_i(\epsilon x, y), \tag{3.6}$$

where $\boldsymbol{u}_{\rm lam}(U_y) = (\partial_y \Psi_{\rm lam}(y), U_y)$ and ϵ is the small parameter.

Since $\partial_y \Psi_0 = 0$ in the limit of $\epsilon \to 0$, we set $\Psi_0 = A(\epsilon x)$. Executing the perturbation expansion with Eq.(3.5) yields

$$\mathcal{L}_y \Psi_i = F_i(\Psi_{\rm lam}, \Psi_0, \cdots, \Psi_{i-1}), \tag{3.7}$$

$$\mathcal{L}_y = \frac{1}{\mathrm{Re}} \partial_y^4 - U_y \partial_y^3, \tag{3.8}$$

for the i-th order of ϵ. We assume that there exists a non-trivial solution of $\mathcal{L}_y \Psi_0^{\rm e} = 0$, then $\Psi_0^{\rm e}$ should be a function independent of y. A necessary condition that each order of Eq.(3.7) has a solution is that the inhomogeneous term of Eq.(3.7) is orthogonal to $\Psi_0^{\rm e}$ as follows:

$$\Psi_0^{\rm e}(X) \int dy F_i(\Psi_{\rm lam}, \Psi_0, \ldots, \Psi_{i-1}) = 0, \tag{3.9}$$

at any $X = \epsilon x$. Substituting Eq.(3.6) into Eq.(3.5) and integrating in y, the condition (3.9) is rewritten as

$$\int dy (\left\{\Psi, \partial_X^2 \Psi\right\}_{Xy} + \frac{\epsilon}{\mathrm{Re}} \partial_X^4 \Psi) = 0, \tag{3.10}$$

for each i because of the periodicity in y. At the zeroth order Eq.(3.10) is automatically satisfied and

$$\Psi_{\rm lam} = -\frac{\rm Re}{Dn}\cos(ny+\theta). \tag{3.11}$$

At the first order

$$\partial_X^3 \int dy \left[-(\partial_y \Psi_L)\Psi_1 + \frac{1}{\rm Re}\partial_X A \right] = 0. \tag{3.12}$$

We assume that $\Psi_1 = ({\rm Re}/D)^2 \partial_X A(X)\sin(ny+2\delta)$, then we obtain the following condition for Reynolds number Re:

$$(1-2n^2U_y^4){\rm Re}^4 - 4U_y^2 n^4 {\rm Re}^2 - 2n^6 = 0. \tag{3.13}$$

Therefore, the condition for Ψ_1 to exist is that Re of Eq.(3.13) is positive real. There exists the following unique real solution of Eq.(3.13):

$${\rm Re} = {\rm Re_l} = \sqrt{\frac{2U_y^2 n^4 + n^3\sqrt{2}}{1-2n^2U_y^4}}, \tag{3.14}$$

when

$$|U_y| < U_y^{\rm c}(n) \equiv \frac{1}{\sqrt[4]{2}\sqrt{n}}. \tag{3.15}$$

This value of Re, $\rm Re_l$, is a likely candidate for the neutral stability curve of the GL state: $\rm Re_c = Re_l(n, U_y)$. In fact, in the case $U_y = 0$, we obtain the same result as the previous works[Siv85, LK14]. Equation (3.14) shows the GL state becomes linearly stable at any Re when $|U_y| > U_y^{\rm c}(n) = (2n^2)^{(-1/4)}$ and thus U_y is a crucial control parameter of 2DKF. We expect this lower bound, i.e., $U_y^{\rm c}(n)$ at $\gamma = 0$ also works at $\gamma > 0$ for most cases.

The stabilization of the GL state for large U_y can be understood as follows. The amplitude of the laminar flow has an upper bound proportional to U_y^{-1}. Thus, for large U_y the amplitude of the GL state is too small to be unstable. In the following numerical experiments in the subcritical regime, we choose $U_y > U_y^{\rm c}$ in order for laminar states to be stable.

3.3.2 Effect of the drag forcing

Next, we check the effect of the drag forcing on coherent structures observed numerically. We focus on the distribution of velocity in the y-direction, since U_y is a conserved quantity and then an effective indicator of the redistribution of the momentum. When γRe is small, the whole state is composed of kink-antikink arrays connecting between adjacent local laminar states with $\beta \neq U_y$ as shown in FIG.3.2a. This state is reminiscent of Cahn-Hilliard like flow emerged at the weakly nonlinear regime for $U_y = 0$ and $\gamma = 0$ where the GL state is linearly unstable for large Re[LK14, HT15]. When γRe is large, the most parts of the whole domain are filled with the GL state and strong vorticity regions emerge spatially-intermittently as shown in FIGs.3.1b and 3.2b. These kinds of structures are strongly connected with the locality of the dynamics of SLT.

To see this connection, we simplify the situation where the whole domain is separated in x-direction into two types of regions in terms of $V(x) = \int_0^{2\pi} dy u_y(x,y)/2\pi$. The first type is a laminar state with the local unit flow rate $V(x) \sim V_0$ which occupies most of the whole domain. The other type is the SLT whose characteristic width is assumed to be $L_{\rm SLT}$. There are N turbulent states, i.e., SLTs. The local unit flow rate of the i-th SLT is V_i which is $V(x)$ averaged over its width. Then, the total flow rate is estimated as follows:

$$U_y L \sim \sum_i^N V_i L_{\rm SLT} + V_0(L - N L_{\rm SLT}), \tag{3.16}$$

where $L = 2\pi/\alpha$ is the width of the box in x direction. When we assume that the turbulence fraction ρ is approximated by $N L_{\rm SLT}/L$, then we obtain the relationship among V_0 and V_i:

$$\sum_{i=1}^N \frac{V_i - V_0}{N} \sim (U_y - V_0)/\rho. \tag{3.17}$$

Since the left-hand side can be regarded as the average distance (norm-like) from the local laminar state and the right-hand side depends on a global quantity ρ, this relationship suggests that the dynamics of SLT directly depends on the number of SLT, N or the turbulence fraction, ρ when $U_y \neq V_0$ for γRe is small. Therefore, the dynamics of SLTs should be nonlocal; they

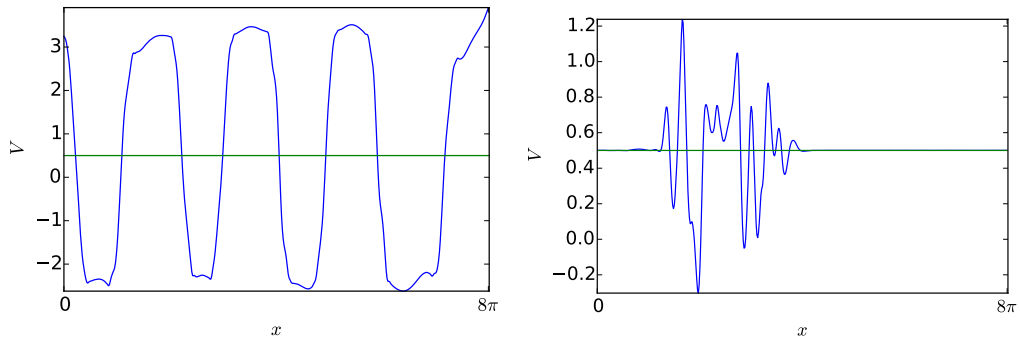

Figure 3.2: Average flow over y direction, $V(x) = \int_0^{2\pi} dy u_y(x,y)/2\pi$ for Re= 240. (a)γRe $= 0$, (b)γRe $= 30$. Straight line ($V = 0.5$) denotes the GL state.

could not decay at a finite turbulence fraction ρ and the whole state could not settle to the global laminar state. We conclude that the condition $V_0 \sim U_y$ should hold for the dynamics of SLT to be local. In this case, a subcritical transition observed in 2DKF belongs to the DP universality class.

3.4 Confirmation of consistency with DP universality class

We numerically conduct quenching experiments and confirm the occurrence of the DP class transition under the conditions that $n = 4$, $U_y = 0.5 > U_y^c(4) \sim 0.42$ and γRe= 30 for two large domains: $1/\alpha = 64$ and 256.

Initial velocity fields are obtained from sustained turbulence consisting of many SLTs at Re= 1000. Then Re is reduced to the target values of Re $\in [230, 250]$. Typically, SLTs create their own replicas and decay to local laminar states randomly and independently.

To define numerically the local turbulence state by the binarization, we adopt the following local distance in a 1D form to the local laminar state denoted by $L_{\rm loc}(x)$:

$$L_{\rm loc}(x) = \frac{1}{2\pi\delta x}\int_0^{2\pi} dy \int_{x-\frac{\delta x}{2}}^{x+\frac{\delta x}{2}} dx'(\omega(x') - \omega_{\rm lam})^2, \tag{3.18}$$

where $\omega_{\rm lam}$ denotes the vorticity of the GL state averaged in y. Then, turbu-

lent states satisfy the condition that $\{x|L_{\rm loc}(x) > \text{const}\}$. Since the threshold constant is not sensitive to the results, we choose $\delta x = \pi/16$ which is comparable to the characteristic width of the typical SLT, $L_{\rm SLT}$. Figure 3.1a shows a typical evolution of turbulent regions defined by this definition. Then, turbulence fraction ρ is defined numerically as

$$\rho = \frac{\alpha}{2\pi}\int_0^{2\pi/\alpha} dx\eta(L_{\rm loc} - C), \tag{3.19}$$

$$\eta(z) = \begin{cases} 1 & (x \geq 0) \\ 0 & (x < 0). \end{cases} \tag{3.20}$$

To characterize some aspects of the DP critical phenomenon observed in our 2D system, we assume direct correspondences between turbulence fraction and each of the order parameters in terms of statistical physics. Based on the standard scaling hypothesis, the process should be invariant under the following rescalings with any b:

$$\epsilon = \frac{\mathrm{Re} - \mathrm{Re_c}}{\mathrm{Re_c}} \to b\epsilon, \tag{3.21}$$

$$\rho \to b^{-\beta}\rho, \tag{3.22}$$

$$x \to b^{-\nu_\perp}x, \tag{3.23}$$

$$t \to b^{-\nu_\parallel}t, \tag{3.24}$$

$$L \to b^{-\nu_\perp}L. \tag{3.25}$$

Hereafter, we use the stationary turbulence fraction, $\rho*$, which is an averaged value of $\rho(t)$ over a long time, and the following values of the indices for (1+1) D DP estimated in ref.[Jen96]: $\beta = 0.276$, $\nu_\perp = 1.097$, $\nu_\parallel = 1.734$, $\mu_\perp = 1.748$ and $\mu_\parallel = 1.841$.

The finite system size scaling Eq.(3.25) is considered because the way of determining $\rho^*(\epsilon)$ is essentially ambiguous both for finite system size and simulation time. Near the critical point $\epsilon \sim 0$, $\rho(t)$ is small and turbulent states should fall into the absorbing state with a finite probability. This means that $\rho^*(\epsilon)$ at a fixed ϵ is monotonically decreasing with increasing the simulation time, and thus it is difficult to confirm the continuity of the transition due to the finite size effect. Figure 3.3(a) shows the turbulence fraction ρ^* for two different system sizes, $\alpha = 1/64$ and $1/256$. The finite size effect is seen especially for $\epsilon < 0$.

To estimate the criticality for an infinite size system, we determine the critical $\mathrm{Re_c}$ in the following way. Focusing on Eqs.(3.21), (3.22) and (3.25), one can obtain the following relations:

$$\rho^*(\epsilon, L) = \epsilon^\beta f(L\epsilon^{\nu_\perp}) = L^{-\frac{\beta}{\nu_\perp}} g(L^{\frac{1}{\nu_\perp}}\epsilon), \tag{3.26}$$

with a universal function f or g. Equation (3.26) means that the function $L^{\beta/\nu_\perp}\rho^*(\epsilon)$ does not depend on the system size L at $\epsilon = 0$. By this fact, $\mathrm{Re_c} = 241$ is estimated as the value of the cross point of the two curves $\rho^*(\epsilon, 128\pi)$ and $\rho^*(\epsilon, 512\pi)$ as shown in FIG.3.3(b). For $\mathrm{Re_c} = 241$, the rescaled functions $L^{\beta/\nu_\perp}\rho^*(\epsilon L^{1/\nu_\perp})$ are collapsed as shown in FIG.3.3(c) as expected by Eq.(3.26). The turbulence fraction ρ^* shown in FIG.3.3(a) is consistent with a continuous transition of (1+1)D DP especially for $\epsilon > 0$. Relatively larger errors are originated from the divergence of longtime correlation at the critical point. For the smaller domain $\alpha = 1/64$, $\rho(t)$ quickly decays to zero for $\epsilon < -0.01$, because large fluctuations cause accidentally transitions into the absorbing state. Note that the existence of a universal function for any system sizes L means that the transition must be continuous for the infinite system size.

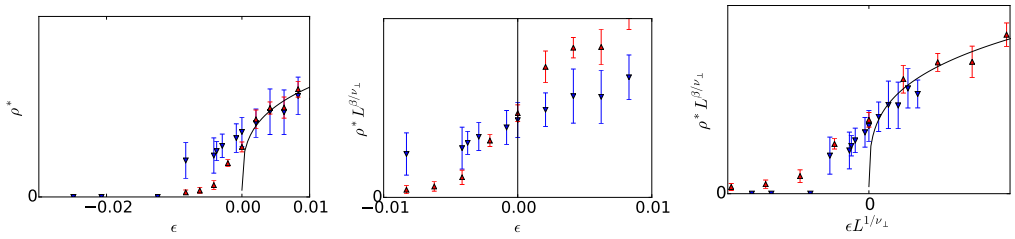

Figure 3.3: (a) Turbulence fraction $\rho^*(\epsilon, L)$, (b)$L^{\beta/\nu_\perp}\rho^*(\epsilon, L)$ and (c) comparison with the universal scaling function $g(L^{\frac{1}{\nu_\perp}}\epsilon)$. Lines indicate prediction of (1+1)D DP. Red upper triangles denote $L = 512\pi$ ($\alpha = 1/256$) and blue lower triangles denote $L = 128\pi$ ($\alpha = 1/64$). Error bars are determined using min-max values.

We also confirm the consistency of two other independent critical exponents, $\mu_\perp$ and $\mu_\parallel$, with those for (1+1)D DP by the distributions of laminar gaps both in space and time shown in FIG.3.4. Note that the indices are

estimated from a single realization with the following scalings relations:

$$N(S_{\rm lam}) \sim S_{\rm lam}^{-\mu_\perp}, \tag{3.27}$$

$$N(T_{\rm lam}) \sim T_{\rm lam}^{-\mu_\parallel}, \tag{3.28}$$

where $N(S_{\rm lam})$ and $N(T_{\rm lam})$ are the histograms of the laminar gaps between turbulent regions in spatial direction $S_{\rm lam}$ and temporal direction $T_{\rm lam}$, respectively.

Each of the two critical exponents, $\mu_\perp$ and $\mu_\parallel$, of the GL state gaps is connected with the fractal box-counting dimension in each direction. Both of the histograms in FIG.3.4 show the consistency with the predictions of DP at relatively longer scales.

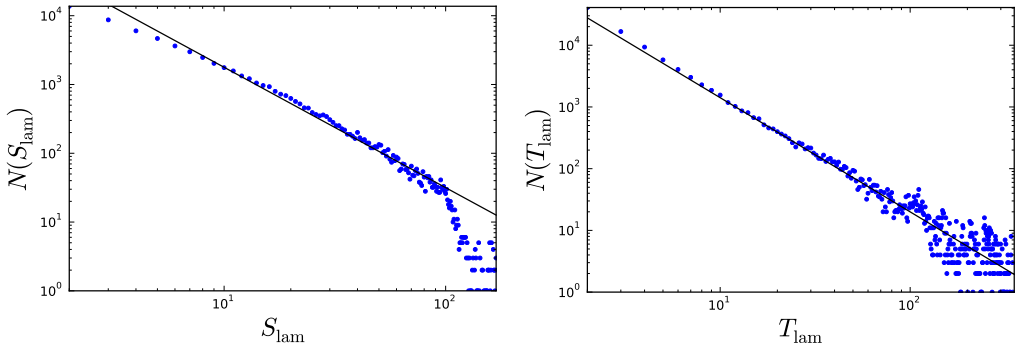

Figure 3.4: Histogram of laminar gaps (a) in spatial direction (b) in temporal direction. Straight lines indicate the predictions of (1+1)D DP.

The time evolutions of the turbulence fraction, $\rho(t)$, for quenching processes are shown in FIG.3.5a. The turbulence fraction decays in power law, $\rho(t) \sim t^{-\alpha}$ ($\alpha = \beta/\nu_\parallel$), in the intermediate stage of the evolution. Finally, ρ falls to a finite value $\rho^*(\epsilon)$ and fluctuate around it.

As shown in FIG.3.5b, by the rescaling with the DP critical exponents, the evolutions of $\rho(t)$ for quenching processes around criticality collapse approximately onto a universal function. The universal functions denoted by F and G are introduced from Eqs.(3.22) and (3.24):

$$\rho(\epsilon, t) = \epsilon^\beta F(t\epsilon^{\nu_\parallel}) = t^{-\frac{\beta}{\nu_\parallel}} G(t^{\frac{1}{\nu_\parallel}}\epsilon). \tag{3.29}$$

All these results support that the subcritical transition observed in 2DKF belongs to (1+1)D DP universality class.

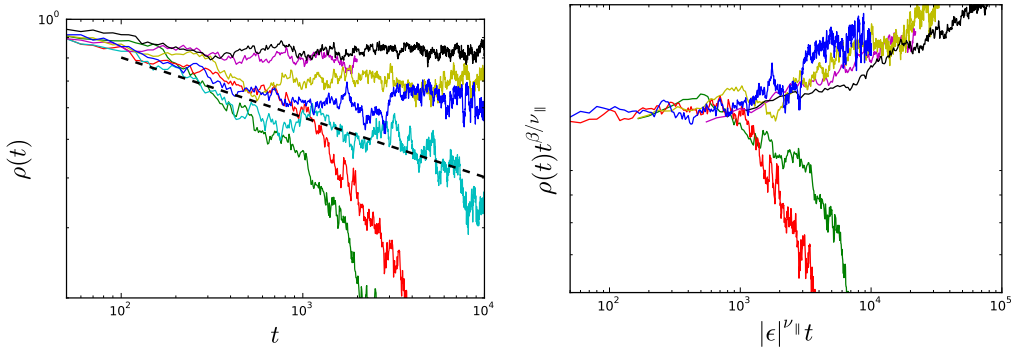

Figure 3.5: (a) Time evolutions of turbulence fraction, $\rho(t)$, for quenching process. Hashed line indicates the prediction of (1+1)D DP. Re $= 239, 240, 241, 242, 243, 245, 247$ from the lower left to the upper right. (b) Estimation of the universal function by rescaling t and ρ with DP exponents. All curves tend to collapse to a single curve if we consider the sign of ϵ. Evolutions near $t \sim 0$ are omitted when correlations with the initial state are strong.

3.5 Concluding remarks

In summary, laminar-turbulence transition belonging to the DP universality class, which is commonly observed in wall-bounded flows with large domains, also occurs in a 2D Kolmogorov flow with periodic boundary conditions. This result clearly shows the concrete forms of driving base shear flow and its inducing local dynamics are not crucial for the occurrence of DP-like subcritical transition. In addition, the DP transition is expected to be realized for a relatively wide range of flows. While the locality of interactions must be also essential for DP, long-range correlations due to the pressure gradient generally present in the Navier-Stakes systems. Thus, our results suggest that the exact correction of the dynamics by coexisting other SLTs is irrelevant to the appearance of the DP class transition. Moreover, we can also conclude the DP class transition realized for subcritical turbulent transition is not universal because transitions different from the DP are observed for 2D Kolmogorov flow with $\gamma = 0$.

The essential characteristics of DP, the existence of the absorbing state and the locality, are related in our system to the flow rate U_y and the drag forcing $-\gamma \boldsymbol{u}$. This parameter dependency is difficult to be identified for wall-

bounded flows since they typically have only one independent parameter Re.

We now consider whether or not there exist in wall-bounded flows or more general flows any counterparts of the roles played by U_y and γ in 2DKF. As discussed above, the drag force can be interpreted as a frictional force due to the walls. From the governing equation (3.1), U_y can be interpreted as an advection speed of a weak disturbance in the frame of zero flow rate: the forcing term is rewritten as $\sin(n(y - U_y t))$ in this frame. For weak localized disturbances or tail parts of SLTs in the zero flow rate frame, which may stay in y-direction, their energy gain oscillates quickly at frequency nU_y and thus is effectively weak. This supports that the global laminar (GL) state is stabilized at large U_y which is also consistent with the fact that the tails of SLT do not develop there [HT15, HT17]. In contrast, a strongly localized disturbance, i.e., SLT that moves with a velocity $-c$ in y-direction in the zero flow rate frame gains kinetic energy efficiently at the frequency $n(U_y - c)$ if the phase velocity c is close to U_y.

The state change in x as shown in Fig.3.2 by introducing γ is also explained as follows: Consider the equation (3.1) with $\partial_y = \partial_x = 0$ that means locally laminar state, no other term than $-\gamma(\boldsymbol{u} - U_y \hat{\boldsymbol{y}})$ exists to determine the absolute value of the laminar state, i.e., local unit flow rate. This means the locally laminar state may not be unique for $\gamma = 0$ while that is unique for $\gamma \gg 1$. Then the realized flows as shown in Fig.3.2 can be "hetero clinic" solution connecting the two laminar states with different unit flow rates for $\gamma = 0$ while only "homoclinic" solution is realized for $\gamma \gg 1$. Moreover, under stick boundary conditions to material walls, the laminar state is unique, and the situation of the transition resembles that of 2D Kolmogorov flow for $\gamma \gg 1$. For the case of Neumann boundary conditions, "homoclinic" solution may disturb the locality of dynamics[CTB17b].

The stable GL state and SLTs might correspond to "bistable" modes in the models of refs[Bar11, Bar16]. Taken into account our results, as shown in Fig.2 there are two types of candidates for a sustaining structure: localized patch and an array of vortex streets with positive or negative signs each of which originates from a kink or an anti-kink of 2DKF. Since the array structure contains energy in longer wavelengths and the drag force makes it decay, only the localized turbulent patch might be sustained. However, the drag force interferes directly with the inverse-transfer. Thus the stronger drag makes SLTs unstable and even annihilated in some situations. This kind of effects also can work in wall-bounded flows but could not be controlled explicitly at fixed Re unlike in 2DKF.

The statistical results might be improved by averaging of additional realizations, but we should mention that separation of time scales between the dynamics of SLT and critical phenomena makes simulation time increase. We should rather emphasize that only a single realization obeys the critical scalings of DP.

An advantage of our system is that the dominant effects can be easily separated in terms of multidimensional parameter space. Therefore we expect that even more general flows share the characteristics of our simple system and that more detailed researches help us to grasp fundamental aspects of sustenance of turbulence.

Effects of global pressure interaction are not observed in the sense of critical phenomenon. We suppose that actually modified dynamics by interaction via pressure is absorbed into a little change for statistical characteristics such as lifetime and splitting time. To confirm the above conjectures, we need to estimate or describe theoretically and quantitatively the interaction or correlation among localised turbulent structures. These estimation and description are important not only for the consideration of minimum elements of the DP transition but also for analyses of collective behaviors of localised turbulent structures which appear as large scale structures such as turbulence stripes in the wall-bounded turbulence[Col65, PGC$^+$02, DSH10, TB11, IDT16].

Chapter 4

General conclusion

4.1 Summery

We have theoretically and numerically investigated 2D Kolmogorov flow focusing on spatially-localized turbulence. Both dynamical and statistical aspects are crucial keys for proper understanding subcritical behavior of turbulence. In Chapter 2, we have found a novel intermittent direction reversal of spatially-localized turbulence, and we have tried to find out the mechanism of direction reversals using a dynamical systems approach in terms of symmetry and invariant solutions in phase space. To describe reversal events, the invariant solutions are still important. In Chapter 3, we have constructed the first Navier-Stokes example to show subcritical transition belonging to DP universality class without mimicking wall-bounded flow. The results support that the concrete form of the dynamics of SLT has only small importance in existence of universal laws. Moreover, it is also clarified that Kolmogorov flow is a fundamental model not only for supercritical turbulence but also for subcritical turbulence.

4.2 Remarks and Future work

The topics of Chapters 2 and 3 have a common point in the sense of the separation of time scales. At a short time scale, their dynamics are complicated and difficult to predict while well-defined states exist on average for moderate time scale, which is the moving direction for Chapter 2 and the number of SLT for Chapter 3. Moreover, at a longer time scale, state transfer between

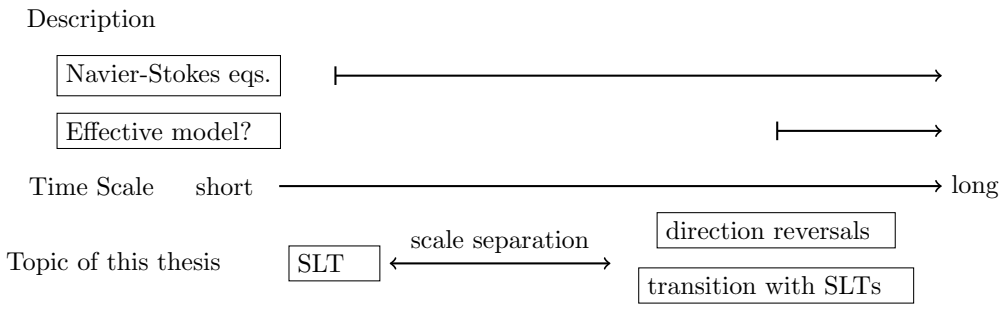

Figure 4.1: Schematic view of scale separation in this thesis.

the well-defined states are observed.

This type of features is shared among a wide range of turbulent systems such as large scale convection (LSC) [Som86, MHFV15] for thermal convection in closed system[SNS$^+$10, NHX15] and multiple states in Taylor-Couette turbulence. Average states, in these cases, at the moderate scale break symmetry to realize anisotropic states. Only a few theories predict statistics of anisotropic states so far. Moreover, scale separation enables us to understand via effective description independent of shorter time scale. This kind of idea supports, for example, Kolmogorov's cascade theory of developed turbulence and effectiveness of the hydrodynamic equations. Constructing statistical theories applicable to scale-separated phenomena of the subcritical regime are future work. As mentioned in Chapter 1 of General introduction, we have not sufficient clues to quantitatively treat "Interaction among other turbulent states".Spatially-localized turbulences behave as they are governed by their own dynamical systems contained in themselves and coupled each other maybe through pressure. Strictly speaking, however, the actual governing equations are global Navier-Stokes equations. We, therefore, should gain a deeper understanding of how such coupled behavior emerges as the solutions of the partial differential equations. Plentiful examples of the interactions between SLTs observed in 2D Kolmogorov flow are presented in Ref.[LK14, HT15]: solitary structures collide or bound to each other. We believe that the works in this thesis are the first step for further study in this direction.

Finally, we emphasize the impact of the introduction of the unit flow rate, $|U_y|$ in this thesis. Originally, Kolmogorov flow was considered in a series of his seminars held in 1958 and 1959 to study "instability" problems of the

laminar flow from the first principle, the Navier-Stokes equations, with mathematical sense[AM60, MS61, Iud65, Arn91]. This model was convenient to find a bifurcation of the laminar flow in the supercritical case, but this original Kolmogorov flow for $U_y = 0$ it was not suitable for subcritical phenomena since the laminar flow should be unstable at low Re. In general, parallel shear profiles in two-dimensional periodic flow should be unstable for some critical amplitude[GYM83, Yam86]. The introduction of $|U_y|$ guarantees that the amplitude of the laminar flow is kept finite even in the limit of infinite Re. This means that the flow is able to be complex with a stable laminar flow. Moreover, this method is easily extended to a wider class of steadily forced flow: introducing the unit flow rate in the direction of explicit coordinate dependence. Thus, we are able to access subcritical phenomena easily. We also hope that this leads to the rigorous proofs and understandings in subcritical transitions.

Bibliography

[AE12] Korinnac T. Allhoff and Bruno Eckhardt. Directed percolation model for turbulence transition in shear flows. *Fluid Dynamics Research*, 44(3):031201, 2012.

[AF00] H Arbell and J Fineberg. Temporally Harmonic Oscillons in Newtonian Fluids. *Physical Review Letters*, 85(4):756–759, 2000.

[AM60] V I Arnold and L D Meshalkin. A.N. Kolmogorov's Seminar on Selected Problems of Analysis (1958/1959). *Uspekhi Mat. Nauk*, 15(1(91)):247–250, 1960.

[AMdL+11] K Avila, D Moxey, A de Lozar, M Avila, D Barkley, and B Hof. The onset of turbulence in pipe flow. *Science*, 333(6039):192–196, 2011.

[AMRH13] M. Avila, F. Mellibovsky, N. Roland, and B. Hof. Streamwise-localized solutions at the onset of turbulence in pipe flow. *Physical Review Letters*, 110(22):1–4, 2013.

[Arn91] V. I. Arnol'd. Kolmogorov's Hydrodynamic Attractors. *Proceedings of the Royal Society A: Mathematical, Physical and Engineering Sciences*, 434(1890):19–22, jul 1991.

[AVOS03] V.S. Anishchenko, T.E. Vadivasova, G.A. Okrokvertskhov, and G.I. Strelkova. Correlation analysis of dynamical chaos. *Physica A: Statistical Mechanics and its Applications*, 325(1-2):199–212, jul 2003.

[Bar11] Dwight Barkley. Simplifying the complexity of pipe flow. *Physical Review E - Statistical, Nonlinear, and Soft Matter Physics*, 84(1):1–8, 2011.

[Bar16] Dwight Barkley. Theoretical perspective on the route to turbulence in a pipe. *Journal of Fluid Mechanics*, 803:P1, 2016.

[BBEC15] Nazmi Burak Budanur, Daniel Borrero-Echeverry, and Predrag Cvitanović. Periodic orbit analysis of a system with continuous symmetry-A tutorial. *Chaos*, 25(7), 2015.

[BCDS15] Nazmi Burak Budanur, Predrag Cvitanović, Ruslan L. Davidchack, and Evangelos Siminos. Reduction of SO(2) symmetry for spatially extended dynamical systems. *Physical Review Letters*, 114(8):1–5, 2015.

[BR11] Piotr Bizoń and Andrzej Rostworowski. Weakly turbulent instability of anti-de Sitter spacetime. *Physical Review Letters*, 107(3):1–4, 2011.

[BSM+15] D Barkley, B Song, V Mukund, G Lemoult, M Avila, and B Hof. The rise of fully turbulent flow. *Nature*, 526(7574):550–553, 2015.

[CH93] M C Cross and P. C. Hohenberg. Pattern formation outside of equilibrium. *Reviews of Modern Physics*, 65(3):851–1112, 1993.

[CK13] Gary J. Chandler and Rich R. Kerswell. Invariant recurrent solutions embedded in a turbulent two-dimensional Kolmogorov flow. *Journal of Fluid Mechanics*, 722:554–595, mar 2013.

[CM88] Hugues Chaté and Paul Manneville. Spatio-temporal intermittency in coupled map lattices. *Physica D: Nonlinear Phenomena*, 32(3):409–422, 1988.

[Col65] Donald Coles. Transition in circular Couette flow. *Journal of Fluid Mechanics*, 21(3):385–425, mar 1965.

[CTB17a] Matthew Chantry, Laurette S. Tuckerman, and Dwight Barkley. Universal continuous transition to turbulence in a planar shear flow. *Journal of Fluid Mechanics*, 824:R1, aug 2017.

[CTB17b] Matthew Chantry, Laurette S. Tuckerman, and Dwight Barkley. Universal continuous transition to turbulence in a planar shear flow. *Journal of Fluid Mechanics*, 824:1–13, 2017.

[DG95] Charles R Doering and J D Gibbon. *Applied Analysis of the Navier-Stokes Equations*. Cambridge Texts in Applied Mathematics. Cambridge University Press, 1995.

[DSH10] Y. Duguet, P. Schlatter, and D. S. Henningson. Formation of turbulent patterns near the onset of transition in plane Couette flow. *Journal of Fluid Mechanics*, 650(August 2016):119–129, may 2010.

[ESHW07] Bruno Eckhardt, Tobias M. Schneider, Bjorn Hof, and Jerry Westerweel. Turbulence Transition in Pipe Flow. *Annual Review of Fluid Mechanics*, 39(1):447–468, 2007.

[Far16] Mohammad Farazmand. An adjoint-based approach for finding invariant solutions of Navier-Stokes equations. *Journal of Fluid Mechanics*, 795:278–312, may 2016.

[Fri95] U Frisch. *Turbulence: The Legacy of A. N. Kolmogorov*. Cambridge University Press, 1995.

[GHC08] J. F. Gibson, J. Halcrow, and P. Cvitanovic. Visualizing the geometry of state space in plane Couette flow. *Journal of Fluid Mechanics*, 611:107–130, sep 2008.

[GY13] Basile Gallet and William R. Young. A two-dimensional vortex condensate at high Reynolds number. *Journal of Fluid Mechanics*, 715:359–388, jan 2013.

[GYM83] Kanefusa Gotoh, Michio Yamada, and Jiro Mizushima. The theory of stability of spatially periodic parallel flows. *Journal of Fluid Mechanics*, 127(-1):45, feb 1983.

[Hin00] Haye Hinrichsen. Non-equilibrium critical phenomena and phase transitions into absorbing states. *Advances in Physics*, 49(7):815–958, 2000.

[Hop48] Eberhard Hopf. A mathematical example displaying features of turbulence. *Communications on Pure and Applied Mathematics*, 1(4):303–322, 1948.

[HT15] Yoshiki Hiruta and Sadayoshi Toh. Solitary solutions including spatially localized chaos and their interactions in two-dimensional Kolmogorov flow. *Physical Review E*, 92(6):063025, dec 2015.

[HT17] Yoshiki Hiruta and Sadayoshi Toh. Intermittent direction reversals of moving spatially localized turbulence observed in two-dimensional Kolmogorov flow. *Physical Review E*, 96(6):063112, dec 2017.

[IDT16] Takahiro Ishida, Yohann Duguet, and Takahiro Tsukahara. Transitional structures in annular Poiseuille flow depending on radius ratio. *Journal of Fluid Mechanics*, 794:R2, may 2016.

[IT01] Tomoaki Itano and Sadayoshi Toh. The Dynamics of Bursting Process in Wall Turbulence. *Journal of the Physical Society of Japan*, 70(3):703–716, 2001.

[Iud65] V I Iudovich. An example of generation of the secondary stationary or periodic flow while loosing the stability by laminar flow of viscous incompressible fluids. *Prikl. Math. Mekh.*, 29:527–544, 1965.

[Jen96] Iwan Jensen. Low-density series expansions for directed percolation on square and triangular lattices. *Journal of Physics A: Mathematical and General*, 29(22):7013–7040, nov 1996.

[Jim90] J Jiménez. The Minimal Channel Flow Unit in Near-Wall Turbulence. *Journal of Fluid Mechanics*, 225:213–240, 1990.

[KE12] Tobias Kreilos and Bruno Eckhardt. Periodic orbits near onset of chaos in plane Couette flow. *Chaos: An Interdisciplinary Journal of Nonlinear Science*, 22(4):047505, dec 2012.

[KK01] Genta Kawahara and Shigeo Kida. Periodic motion embedded in plane Couette turbulence: regeneration cycle and burst. *Journal of Fluid Mechanics*, 449:291, 2001.

[KKS+16] T. Khapko, T. Kreilos, P. Schlatter, Y. Duguet, B. Eckhardt, and D. S. Henningson. Edge states as mediators of bypass

transition in boundary-layer flows. *Journal of Fluid Mechanics*, 801:R2, aug 2016.

[KM80] Robert H Kraichnan and David Montgomery. Two-dimensional turbulence. *Reports on Progress in Physics*, 43(5):547–619, may 1980.

[Kra67] Robert H. Kraichnan. Inertial Ranges in Two-Dimensional Turbulence. *Physics of Fluids*, 10(7):1417, 1967.

[KT05] Michikazu Kobayashi and Makoto Tsubota. Kolmogorov Spectrum of Quantum Turbulence. *Journal of the Physical Society of Japan*, 74(12):3248–3258, dec 2005.

[KUvV12] Genta Kawahara, Markus Uhlmann, and Lennaert van Veen. The Significance of Simple Invariant Solutions in Turbulent Flows. *Annual Review of Fluid Mechanics*, 44(1):203–225, 2012.

[KZE14] Tobias Kreilos, Stefan Zammert, and Bruno Eckhardt. Comoving frames and symmetry-related motions in parallel shear flows. *Journal of Fluid Mechanics*, 751:685–697, jul 2014.

[Lam45] H Lamb. *Hydrodynamics*. Dover Books on Physics. Dover publications, 1945.

[Lan44] L. D. Landau. On the problem of turbulence. *Dokl. Akad. Nauk SSSR*, 44(8):339–349, 1944.

[LBF+14] Jason Laurie, Guido Boffetta, Gregory Falkovich, Igor Kolokolov, and Vladimir Lebedev. Universal Profile of the Vortex Condensate in Two-Dimensional Turbulence. *Physical Review Letters*, 113(25):254503, dec 2014.

[LK14] Dan Lucas and Rich R. Kerswell. Spatiotemporal dynamics in two-dimensional Kolmogorov flow over large domains. *J. Fluid Mech*, 750(1993):518–554, 2014.

[LK15] Dan Lucas and Rich R. Kerswell. Recurrent flow analysis in spatiotemporally chaotic 2-dimensional Kolmogorov flow. *Physics of Fluids*, 27(4):045106, apr 2015.

[LL59] L D Landau and E M Lifshitz. *Course of theoretical physics. vol. 6: Fluid mechanics*. London, 1959.

[Lor63] Edward N. Lorenz. Deterministic Nonperiodic Flow. *Journal of the Atmospheric Sciences*, 20(2):130–141, mar 1963.

[LSA+16a] Grégoire Lemoult, Liang Shi, Kerstin Avila, Shreyas V. Jalikop, Marc Avila, and Björn Hof. Directed percolation phase transition to sustained turbulence in Couette flow. *Nature Physics*, 12(3):254–258, feb 2016.

[LSA+16b] Grégoire Lemoult, Liang Shi, Kerstin Avila, Shreyas V Jalikop, Marc Avila, and Björn Hof. Directed percolation phase transition to sustained turbulence in Couette flow. *Nature Physics*, 12(March):254–258, feb 2016.

[Mar87] C. Marchioro. An example of absence of turbulence for any Reynolds number: II. *Communications in Mathematical Physics*, 108:647–651, 1987.

[MD93] F. Melo and S. Douady. From solitary waves to static patterns via spatiotemporal intermittency. *Physical Review Letters*, 71(20):3283–3286, nov 1993.

[MD15] Sergio E. Mangioni and Roberto R. Deza. Stochastic dissipative solitons. *Physical Review E*, 92(3):032116, 2015.

[ME12] F. Mellibovsky and B. Eckhardt. From travelling waves to mild chaos: a supercritical bifurcation cascade in pipe flow. *Journal of Fluid Mechanics*, 709:149–190, 2012.

[MHFV15] Pankaj Kumar Mishra, Johann Herault, Stephan Fauve, and Mahendra K. Verma. Dynamics of reversals and condensates in two-dimensional Kolmogorov flows. *Physical Review E*, 91(5):1–12, 2015.

[MS61] L.D. Meshalkin and Ia.G. Sinai. Investigation of the stability of a stationary solution of a system of equations for the plane movement of an incompressible viscous liquid. *Journal of Applied Mathematics and Mechanics*, 25(6):1700–1705, jan 1961.

[MW66] N. D. Mermin and H. Wagner. Absence of ferromagnetism or antiferromagnetism in one- or two-dimensional isotropic Heisenberg models. *Physical Review Letters*, 17(22):1133–1136, 1966.

[Nag90] M. Nagata. Three-dimensional finite-amplitude solutions in plane Couette flow: bifurcation from infinity. *Journal of Fluid Mechanics*, 217(-1):519, aug 1990.

[NDL17] Shreyas Acharya Neelavara, Yohann Duguet, and François Lusseyran. State space analysis of minimal channel flow. *Fluid Dynamics Research*, 49(3):035511, jun 2017.

[NHX15] Rui Ni, Shi-Di Huang, and Ke-Qing Xia. Reversals of the large-scale circulation in quasi-2D RayleighBénard convection. *Journal of Fluid Mechanics*, 778:R5, 2015.

[PGC+02] Arnaud Prigent, Guillaume Grégoire, Hugues Chaté, Olivier Dauchot, and Wim van Saarloos. Large-Scale Finite-Wavelength Modulation within Turbulent Shear Flows. *Physical Review Letters*, 89(1):014501, 2002.

[Pom86] Y. Pomeau. Front motion, metastability and subcritical bifurcations in hydrodynamics. *Physica D: Nonlinear Phenomena*, 23(1-3):3–11, 1986.

[Rey83] O. Reynolds. An Experimental Investigation of the Circumstances Which Determine Whether the Motion of Water Shall Be Direct or Sinuous, and of the Law of Resistance in Parallel Channels. *Philosophical Transactions of the Royal Society of London*, 174(0):935–982, 1883.

[RT71] David Ruelle and Floris Takens. On the nature of turbulence. *Communications in Mathematical Physics*, 20(3):167–192, 1971.

[SFB16] Vishwanath Shukla, Stephan Fauve, and Marc Brachet. Statistical theory of reversals in two-dimensional confined turbulent flows. *Physical Review E*, 94(6):061101, dec 2016.

[SHG16] Hong Yan Shih, Tsung Lin Hsieh, and Nigel Goldenfeld. Ecological collapse and the emergence of travelling waves at the onset of shear turbulence. *Nature Physics*, 12(3):245–248, 2016.

[Siv85] Gregory I. Sivashinsky. Weak turbulence in periodic flows. *Physica D: Nonlinear Phenomena*, 17(2):243–255, 1985.

[SMDK14] Masaki Shimizu, Paul Manneville, Yohann Duguet, and Genta Kawahara. Splitting of a turbulent puff in pipe flow. *Fluid Dynamics Research*, 46(6):061403, dec 2014.

[SNS+10] Kazuyasu Sugiyama, Rui Ni, Richard J A M Stevens, Tak Shing Chan, Sheng Qi Zhou, Heng Dong Xi, Chao Sun, Siegfried Grossmann, Ke Qing Xia, and Detlef Lohse. Flow reversals in thermally driven turbulence. *Physical Review Letters*, 105(3):1–4, 2010.

[Som86] J Sommeria. Experimental study of the two-dimensional inverse energy cascade in a square box. *Journal of Fluid Mechanics*, 170:139, 1986.

[ST16] Masaki Sano and Keiichi Tamai. A universal transition to turbulence in channel flow. *Nature Physics*, 12(3):249–253, feb 2016.

[STGS17] Balachandra Suri, Jeffrey Tithof, Roman O. Grigoriev, and Michael F. Schatz. Forecasting Fluid Flows Using the Geometry of Turbulence. *Physical Review Letters*, 118(11):114501, mar 2017.

[STM+14] Balachandra Suri, Jeffrey Tithof, Radford Mitchell, Roman O. Grigoriev, and Michael F. Schatz. Velocity profile in a two-layer Kolmogorov-like flow. *Physics of Fluids*, 26(5), 2014.

[TB11] Laurette S. Tuckerman and Dwight Barkley. Patterns and dynamics in transitional plane Couette flow. *Physics of Fluids*, 23(4):041301, 2011.

[TFY17] Makoto Tsubota, Kazuya Fujimoto, and Satoshi Yui. Numerical Studies of Quantum Turbulence. *Journal of Low Temperature Physics*, 188(5-6):119–189, 2017.

[TI05] Sadayoshi Toh and Tomoaki Itano. Interaction between a large-scale structure and near-wall structures in channel flow. *Journal of Fluid Mechanics*, 524(C):249–262, 2005.

[TIMO14] M. Tarama, Y. Itino, A. M. Menzel, and T. Ohta. Individual and collective dynamics of self-propelled soft particles. *European Physical Journal: Special Topics*, 223(1):121–139, 2014.

[TKCS07] Kazumasa A. Takeuchi, Masafumi Kuroda, Hugues Chaté, and Masaki Sano. Directed Percolation Criticality in Turbulent Liquid Crystals. *Physical Review Letters*, 99(23):234503, 2007.

[TKCS09] Kazumasa A. Takeuchi, Masafumi Kuroda, Hugues Chaté, and Masaki Sano. Experimental realization of directed percolation criticality in turbulent liquid crystals. *Physical Review E*, 80(5):051116, nov 2009.

[TT95] John Toner and Yuhai Tu. Long-range order in a two-dimensional dynamical XY model: How birds fly together. *Physical Review Letters*, 75(23):4326–4329, 1995.

[TT14] Toshiki Teramura and Sadayoshi Toh. Damping filter method for obtaining spatially localized solutions. *Physical Review E*, 89(5):052910, may 2014.

[TT16] Toshiki Teramura and Sadayoshi Toh. Chaotic self-sustaining structure embedded in the turbulent-laminar interface. *Physical Review E*, 93(4):1–5, 2016.

[VCBJ+95] Tamas Vicsek, Andras Czirok, Eshel Ben-Jacob, Inon Cohen, and Ofer Shochet. Novel Type of Phase Transition in a System of Self-Driven Particles. *Physical Review Letters*, 75(6):1226–1229, aug 1995.

[VEE+17] Eliott Varon, Yoann Eulalie, Stephie Edwige, Philippe Gilotte, and Jean-Luc Aider. Chaotic dynamics of large-scale structures in a turbulent wake. *Physical Review Fluids*, 2(3):034604, mar 2017.

[VZ12] Tamás Vicsek and Anna Zafeiris. Collective motion. *Physics Reports*, 517(3-4):71–140, 2012.

[Wal97] Fabian Waleffe. On a self-sustaining process in shear flows. *Physics of Fluids*, 9(4):883–900, 1997.

[WCA13] A. P. Willis, P Cvitanović, and M Avila. Revealing the state space of turbulent pipe flow by symmetry reduction. *Journal of Fluid Mechanics*, 721:514–540, apr 2013.

[WPKM08] A.P Willis, J Peixinho, R.R Kerswell, and T Mullin. Experimental and theoretical progress in pipe flow transition. *Philosophical Transactions of the Royal Society A: Mathematical, Physical and Engineering Sciences*, 366(1876):2671–2684, aug 2008.

[WSC16] Ashley P. Willis, Kimberly Y. Short, and Predrag Cvitanović. Symmetry reduction in high dimensions, illustrated in a turbulent pipe. *Physical Review E - Statistical, Nonlinear, and Soft Matter Physics*, 93(2):1–5, 2016.

[Yam86] Michio Yamada. Nonlinear Stability Theory of Spatially Periodic Parallel Flows. *Journal of the Physical Society of Japan*, 55(9):3073–3079, 1986.

Appendix A

Numerical method

A.1 Pseudospectral method

The governing equation to be integrated numerically is the equation for the vorticity $\omega = \boldsymbol{\nabla} \times \boldsymbol{u}$,

$$\partial_t \omega + (\boldsymbol{u} \cdot \boldsymbol{\nabla})\omega = -\gamma\omega + \frac{1}{\mathrm{Re}}\nabla^2\omega + f_\omega, \tag{A.1}$$

where $f_\omega = \boldsymbol{\nabla} \times \boldsymbol{f}$.

The vorticity ω is expanded using the Fourier series as follows:

$$\omega(x, y) = \sum_{k=Nx/2}^{Nx/2} \sum_{l=-Ny/2}^{Nx/2} \hat{\omega}(k, l) \exp(i\alpha kx + ily). \tag{A.2}$$

Since the vorticity ω takes a real value, the condition $\hat{\omega}(-k, -l) = \hat{\omega^*}(k, l)$ holds.

Here, the asterisk denotes complex conjugate. The governing equations for the coefficients are derived using the pseudo-spectral method:

$$\frac{d}{dt}\hat{\omega}(k, l) = \mathcal{L}(k, l)\hat{\omega}(k, l) + \mathcal{F}, \tag{A.3}$$

$$\mathcal{L}(k, l) = -\gamma - \frac{\alpha^2 k^2 + l^2}{\mathrm{Re}}, \tag{A.4}$$

$$\mathcal{F} = \mathrm{FFT}(-(\boldsymbol{u} \cdot \boldsymbol{\nabla})\omega + f_\omega). \tag{A.5}$$

Here, the nonlinear term are calculated using Fast Fourier Transform(FFT), and dealiased by the two-thirds rule. The velocity $\boldsymbol{u}$ with the unit flow rate U_y is calculated via the periodic stream function ψ as follows:

$$\hat{\psi}(k,l) = \frac{\hat{\omega}(k,l)}{\alpha^2 k^2 + l^2} \ (k \neq 0, l \neq 0), \tag{A.6}$$

$$\hat{u_x}(k,l) = il\hat{\psi}(k,l), \tag{A.7}$$

$$\hat{u_y}(k,l) = -ik\hat{\psi}(k,l) + U_y. \tag{A.8}$$

Note that the value of $\hat{\psi}(0,0)$ does not affect the results.

A.2 Avoiding stiffness from viscos term

Straight forward explicit scheme for Eq.(A.3) needs a small time-step dt for high resolution simulation since linear term of Eq.A.4 has the viscoss term proportional to $\alpha^2 k^2 + l^2$. In order to solve such a *stiff* equation, we derive a numerical scheme to solve the linear term exactly as follows. First, keeping in mind the exact solution of the linear equation, we consider new variable

$$\hat{\Omega}(k,l) = \hat{\omega}(k,l)\exp(\mathcal{L}(k,l)t). \tag{A.9}$$

The evolution of the new variable $\hat{\Omega}$ obeys the following equation:

$$\frac{d}{dt}\hat{\Omega}(k,l) = \exp(\mathcal{L}(k,l)t)\mathcal{F}(\omega(t)). \tag{A.10}$$

Applying the Heun (2nd order Runge-Kutta) method with a time step, Δt, to the evolution equation (A.10) the following formal scheme is obtained:

$$k_1 = \exp(\mathcal{L}(k,l)t)\mathcal{F}(\omega(t)), \tag{A.11}$$

$$k_2 = \exp(\mathcal{L}(k,l)(t+\Delta t))\mathcal{F}(\omega(t) + \exp(-\mathcal{L}(k,l)t)k1\Delta t), \tag{A.12}$$

$$\Omega(t+\Delta t) = \Omega(t) + \Delta t(k_1 + k_2), \tag{A.13}$$

$$\omega(t+\Delta t) = \exp(-\mathcal{L}(k,l)\Delta t)\omega(t) + \frac{\exp(-\mathcal{L}(k,l)(t+\Delta t))}{2}\Delta t(k_1 + k_2). \tag{A.14}$$

Omitting unnecessary operations, one can finally obtain the numerical scheme for ω

$$k_1^{'} = \mathcal{F}(\omega(t)), \tag{A.15}$$

$$k_2^{'} = \exp(-\mathcal{L}(k,l)\Delta t)\mathcal{F}(\omega(t) + k1\Delta t), \tag{A.16}$$

$$\omega(t+\Delta t) = \exp(-\mathcal{L}(k,l)\Delta t)(\omega(t) + \frac{k_1^{'}\Delta t}{2}) + \frac{k_2^{'}\Delta t}{2}. \tag{A.17}$$

Since in this scheme the large $\mathcal{L}(k,l)\Delta t$ terms only appear as the argument of the exponential function with minus sign, the stiffess of the original scheme is removed.

A.3 Newton method

We use Newton method to obtain an exact invariant solution with the iterative method and without any direct calculation of component of linearized matrix $DF(\boldsymbol{X})$.

The $(n+1)$th solution of Newton iteration, $\boldsymbol{X}_{n+1}$, follows

$$DF(\boldsymbol{X}_n)\delta\boldsymbol{X} = -\boldsymbol{F}(\boldsymbol{X}_n), \tag{A.18}$$

$$\delta\boldsymbol{X} = \boldsymbol{X}_{n+1} - \boldsymbol{X}_n. \tag{A.19}$$

Thus, we should solve the following linear problem:

$$A\boldsymbol{X} = \boldsymbol{b}, \tag{A.20}$$

where $A = DF(\boldsymbol{X}_n)$ and $b = -\boldsymbol{F}(\boldsymbol{X}_n)$. GMRES(Generel Minimal RESisual) method find a solution $\boldsymbol{X}$ which minimize the residual r

$$r = ||A\boldsymbol{X} - \boldsymbol{b}||, \tag{A.21}$$

of linear equation $A\boldsymbol{X} = \boldsymbol{b}$ on the Krylov space $\mathcal{K}_n = \mathrm{Span}(b, A\boldsymbol{b}, \ldots, A^{n-1}\boldsymbol{b})$. Using Gram-Schmidt iteration, the Krylov space$\mathcal{K}_n$ is constructed:

$$\boldsymbol{v}_1 = \frac{\boldsymbol{b}}{|\boldsymbol{b}|}, \tag{A.22}$$

$$\hat{\boldsymbol{v}}_{i+1} = A\boldsymbol{v}_i - \sum_j^i \boldsymbol{v}_j \boldsymbol{v}_j^{\mathrm{T}} A\boldsymbol{v}_i, \tag{A.23}$$

$$\boldsymbol{v}_i = \frac{\hat{\boldsymbol{v}}_i}{|\hat{\boldsymbol{v}}_i|}. \tag{A.24}$$

In the n iterative step, Hessenberg matrix $H_{n+1,n}$ is defined

$$AV_n = V_{n+1}H_{n+1,n}, \tag{A.25}$$

using V_n, which is the matrix with coluumns $\boldsymbol{v}_1, \cdots, \boldsymbol{v}_n$. Note that V_n connects the components of an element in Krylov space $\mathcal{K}_n$ and original one. The residual r is rewriten as,

$$r = ||A\boldsymbol{X} - \boldsymbol{b}|| = ||H_{n+1,n}\boldsymbol{Y} - |\boldsymbol{b}|\boldsymbol{e}_1||, \tag{A.26}$$

where $\boldsymbol{X} = V_n\boldsymbol{Y}$ and $\boldsymbol{e}_1 = (1, 0, \ldots, 0)$. The solution is obtained in the Krylov space using QR decomposition of $H_{n+1,n}$ using Givens rotation. Then, we reduce the order of the matrix from N to n, where the residual is smaller than the toerance.

Moreover, we do not need to refer to elements of the linearized matrix since we calculate

$$DF(\boldsymbol{X}_n)\delta\boldsymbol{X} \sim \frac{\boldsymbol{F}(\epsilon\delta\boldsymbol{X} + \boldsymbol{X}_n) - \boldsymbol{F}(\boldsymbol{X}_n)}{\epsilon}, \tag{A.27}$$

using a small constant ϵ.